Fluid Flow Analysis of a Turbulent Offset Jet Impinging on a Wavy Wall Surface

Tej Pratap Singh[1], Amitesh Kumar[2,*], and Ashok Kumar Satapathy[1]
[1]Department of Mechanical Engineering
National Institute of Technology, Rourkela 769008, India
[2]Department of Mechanical Engineering
Indian Institute of Technology (BHU), Varanasi 221005, India

June 26, 2019

Abstract

The fluid flow characteristics of a turbulent offset jet impinging on a wavy wall surface has been investigated numerically. Two-dimensional Reynolds averaged Navier-Stokes (RANS) equations are solved by the Finite Volume Method (FVM). In the governing differential equations, the convective and diffusive terms are discretised by the power law upwind scheme and second order central difference respectively. The Semi-Implicit Method for Pressure Linked Equation (SIMPLE) algorithm is utilised to link the pressure to the velocity. The offset ratio is set to 7.0 and the Reynolds number is fixed to $15,000$. The width of the jet is taken as the characteristic length. The amplitude of the wavy wall surface is varied from 0.1 to 0.7 with an interval of 0.1 and the number of cycle is fixed to 10. The results of fluid flow and turbulent characteristics of the offset jet are presented in the form of contours of streamline, velocity vector, turbulent kinetic energy, dissipation rate, pressure and Reynolds shear stress. The variation in integral constant of momentum flux, wall shear stress and pressure along the wall is presented and compared also. The decay in maximum streamwise velocity in downstream direction and jet half-width along streamwise direction are also presented and discussed. The wavy surface introduces some remarkable features which are not present in a normal plane wall case. These features have been discussed in detail.

Keywords: Amplitude, Numerical simulation, Offset jet, Turbulent flow, Wavy wall.

Nomenclature

$C_{1\epsilon}$, $C_{2\epsilon}$, C_μ	turbulence model constants
a	width of the jet
D	distance between the wall jet and offset jet
G	production by shear
P	non-dimensional static pressure
$\bar{p}$	static pressure
$\overline{p_0}$	ambient pressure
Re	Reynolds number, $U_0 a/\nu$
U_0	average inlet jet velocity
U_{max}	non-dimensional maximum streamwise velocity
$\bar{x}$, $\bar{y}$	dimensional co-ordinates
X, Y	non-dimensional co-ordinates
$\bar{u}$, $\bar{v}$	dimensional velocities in x, y -directions respectively
U, V	non-dimensional velocities in X, Y -directions respectively
u_τ	non-dimensional friction velocity, $\sqrt{(\nu_t\,(\partial u_L/\partial y_n)_{wall})}$
y^+	non-dimensional co-ordinate, $y u_\tau/\nu$
$Y_{0.5}$	non-dimensional distance in the cross-streamwise direction at which $U = 1/2 \times U_{max}$

*email: amitesh.mec@iitbhu.ac.in

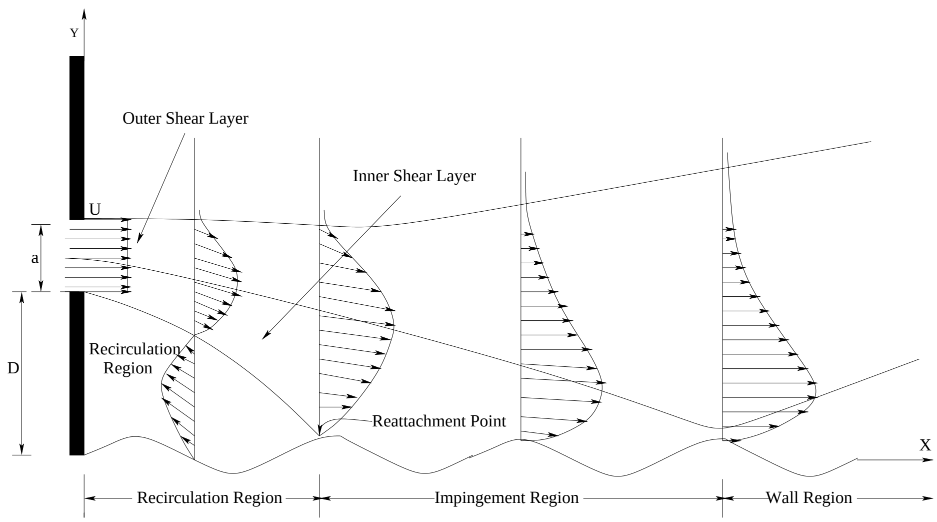

Figure 1: Schematic diagram of turbulent offset jet impinging on a wavy suface

Greek symbols

ε_n	rate of dissipation
k_n	turbulent kinetic energy, $= \frac{1}{2}(\overline{u'^2} + \overline{v'^2})/U_0^2$
ν, ν_t	laminar and turbulent kinematic viscosity
σ_k, σ_ε	turbulent model constant
$\tau_{w,n}$	non-dimensional wall shear stress
C_{pw}	wall static pressure coefficient

Subscripts

n	non-dimensional
vc	vortex center
max	maximum
min	minimum

1 Introduction

The turbulent jets are widely used in many industrial and engineering applications like fuel injection system, burners, gas turbine combustors, boilers, cooling of turbine blade in gas turbine, electronic components and thrust augmentation in air craft during vertical take-off. When turbulent jet is discharged into the surrounding medium, its characteristics basically depend~~s~~ upon the three main factors like: shape and size of the nozzle, height of the nozzle from the base and the surrounding medium. Surrounding medium may be moving or stationary depending upon the practical applications. Turbulent jets are characterised as the wall bounded jet and free jet. The wall bounded jets are wall jet, offset jet and a wall jet with a parallel offset jet (i.e., dual jet). The different types of turbulent jets are thoroughly explained by ~~the~~ Rajarathnam [1]. ~~When the wall is present with the jet, the behaviour of the turbulent jet changes.~~ In the several wall bounded turbulent jets mentioned earlier, the offset turbulent jet plays more vital role in practical engineering applications. Due to this, many researchers [2, 3, 4, 5, 6, 7, 8, 9] have focused their ~~there~~ attention on unfolding its characteristics. Recently, Castro and Demuren [10] studied the flow characteristics for both non rotating and rotating pipe and jet flow using large eddy simulation. They used three Reynolds number 5300, $12,000$ and $24,000$ and four swirl rates 0, 0.5, 1 and 2. They noticed that by increasing the swirl of the jet the component of axial turbulent intensity increases.

The offset jet may be defined as a jet placed with some offset distance from the wall. The offset ratio (OR) is defined as the ratio of the offset distance (D) to the jet width (a), i.e. $OR = D/a$. The schematic diagram of the turbulent offset jet impinging on a wavy surface is shown in figure1. Due to the presence of the wall, the pressure difference occurs between above and below of the jet. The low atmospheric pressure zone is created ~~between below the jet and above the wall~~ between the jet and the wall. As a result, the jet tilts towards the wall and the inner shear layer of the offset jet strikes to the wall. This effect is known as the "Coanda effect"[11]. The point of interaction with the wall is termed as the reattachment point. The region between the below jet and the reattachment point is known as the recirculation region. After the jet strikes the plate, the fluid changes the flow direction. The region, after the reattachment point in the downstream direction, is known as the impingement region. Further, the jet in the downstream direction behaves like a wall jet. There are so many experimental techniques to examine the physical behaviour of the turbulent offset jet. The first experimental study on offset jet was provided by Sawyer [12], ~~experimentally~~ who examined the effect of cavity length and cavity pressure of an offset jet in the ~~converging~~impingement region. He did the detailed analysis of the velocity and pressure, and mentioned that the growth rate of a curved jet is similar to the growth rate of a plane jet [13]. Later study provided~~. After that he~~ ~~modifying his analysis~~ ~~[13]~~ ~~modified his analysis and~~ ~~the researcher mentioned that the new results provide~~ the good prediction of the averege pressure and recirculation region length. Bourque and Newman [2] used pressure tap as the~~a~~ measurement technique. They varied ~~used~~ Reynolds number (Re) and offset ratio (h/w) from ~~between~~ $2760-7750$~~.~~ and ~~They varied the offset ratio (h/w) from~~ $4-48.5$ respectively where, h is the offset distance and w is the nozzle width. Bourque and Newman [2] studied ~~They studied~~ the effect of the offset ratio and the Reynolds number with the axial distance of the reattachment point. The experimental study showed that~~They also examined~~ the low atmospheric pressure in the recirculation region~~s~~ is found. Afterwa~~o~~rds, Lund [4] used the same experimental method to find out the wall static pressure and the reattachment length. The investigator used~~He considered~~ the Reynolds number equal to $20,000$ and the offset ratio in between 0.694 to 21.8 and noticed that the trajectory of jet center line opposes the trend of the arc of a circle. Rajaratnam and Subramanya [14] adopted the Prandtl type Pitot static tube screwdriver probe and piezometer holes as the experimental techniques to study the static pressure and mean velocity in the ~~converging~~impingement region and the wall jet regions. They used Reynolds number (Re) equal to $71,000$ and the offset ratio up to 6.5. To examine the static pressure in ~~converging~~impingement region, an experimental investigation using ~~Hoch and Jiji~~ pressure tap and single hot wire was performed [3]. They considered Reynolds number and offset ratio of $16,000$ and $3-8.7$ respectively for this study. The experimental study concluded~~s~~ that ~~considered pressure tap and single hot wire as experimental techniques and examined~~ the static pressure in ~~converging~~impingement zone, the velocity decay, and the reattachment length were affected by the secondary free stream velocity. ~~They used Reynolds number 16,000 for the offset ratio of 3 to 8.7. Rajaratnam and Suramanya [14] adopted the Prandtl type Pitot static tube screwdriver probe and piezometer holes as the experimental techniques to study the static pressure and mean velocity in the converging region and the wall jet regions. They used Reynolds number (Re) equal to 71,000 and the offset ratio up to 6.5.~~ Pelfrey and Liburdy [15] used one-component Laser Doppler Anemometer (LDA) system to examine the turbulent characteristics of the offset jet. They studied the turbulence intensities and the mean velocity flow fields in the ~~converging~~impingement regions. The~~y~~ researchers used Reynolds number (Re) and the offset ratio (h/w) equal to $15,000$ and 7, respectively. They defined the offset ratio as the ratio of offset distance (h) from the jet centre line to the bottom wall with jet width (w). In addition, they also noticed~~found out~~ the large strain rate due to the presence of jet curvature [6]. Nasr and Lai [16] also defined the offset jet in a similar manner as defined by Pelfrey and Liburdy [15]. Nasr and Lai~~They~~ used small offset ratio (h/w) equals to2.125 and the two-component Laser Doppler Anemometer (LDA) as the experimental technique. For the modelling part, they used three numerical techniques: standard $k-\varepsilon$, RNG model and Reynolds stress model~~. They~~ and compared the numerical results with the LDA experimental results. ~~and~~It was concluded that out of three mentioned numerical models, standard $k-\varepsilon$ model provided~~s~~ the better solution. Launder and Spalding [17] provided the concept of $k-\varepsilon$ turbulence model to study the complex behavior of the turbulent jet near the adjacent surface and phenomena of free shear flow. They [17] noticed that ~~this~~The $k-\varepsilon$ turbulence model provided~~s~~ the more accurate prediction near the recirculation region. Benim and Zinser [18] also used finite element method to study the turbulent flow. They examined the behavior of flow characteristics near the wall region. They estimated the wall shear stress and provided its importance in viscous sub layer region.

Koo and Park [19] used QUICKER scheme to solve the turbulent flow on a non-uniform rectangular grid domain. They did the comparison between QUICKER scheme, hybrid scheme and Skew-upwind scheme and showed their results in the form of maximum velocity decay, streamlines, velocity profiles and shear stress distribution. ~~In recent study, Fu et al. [20] showed studied the efficacy of RANS equations for a wall jet and low offset ratios (i.e., 0.5, 1, 1.5 and 2). They noticed that the wall function approach needs to be refined~~

~~to get reliable prediction for wall normal component. Koo and Park [19] used QUICKER scheme to solve the turbulent flow on a non-uniform rectangular grid domain. They did the comparison between QUICKER scheme, hybrid scheme and Skew-upwind scheme and showed their results in the form of maximum velocity decay, streamlines velocity profiles and shear stress distribution.~~

Numerical analysis of impinging turbulent jet on a flat surface is also one of the important research areas with different structure which is mainly used in various engineering applications like vectoring fighter planes and take off and landing of a VTOL aircraft. The two-dimensional single impinging jet was studied by Chuang [21]. They used $k-\varepsilon$ two-equations turbulence model to examine the flow behavior of a turbulent jet. Further, Chuang and Wei [22] used same numerical method to investigate the two-dimensional oblique impinging jet on a plane surface. They used SIMPLE-C algorithm to link the pressure to the velocity. They concluded that as the inclination of impinging jet reduces the maximum pressure zone shifts towards the left side of~~n~~ the domain. The two-dimensional twin impinging jet with cross flow was studied by Chuang et al. [23], both theoretically and numerically by using two-equation $k-\varepsilon$ turbulence model given by Jones and Launder . They stated that as the cross flow increases the lift force of the air craft reduces. The thermal characteristics of a smooth plane maintained at a constant heat flux was investigated using hot wire anemometer [24]. The spacing between a single axisymmetric jet and impingement plate was changed~~ranged~~ from 1 to 8 of nozzle diameter and observed that maximum heat transfer occurs when the length between the jet and impingement plate is equal to jet diameter. Nanofluids also play an important role in heat transfer applications of impingement jet. It is studied that for 6% of the volume fraction of nanofluid, the heat transfer coefficient increases almost 22% in impingement jet as compared to the base fluid (i.e. water) having equal Reynolds number and equal inlet velocity [25].

Many of the researchers [26, 27, 28, 29, 7, 9, 30] have also examined the thermal characteristics of the offset jet with different offset ratios. Holland and Liburdy [27] performed the experimental work and used similar flow structure as considered by Pelfry and Liburdy [6] and studied the heat transfer characteristics of the heated offset jet which impinges on an adiabatic plane wall. They summarized~~rmised~~ that thermal distribution depends on the offset ratio and flow curvature increases with higher offset ratio. V~~i~~shnuvardhanarao and Das [26] also considered the offset distance (h) from the jet centre line and studied the heat transfer for the offset ratio of 3, 7, and 11. They calculated the Reynolds number based on the jet inlet velocity (U_0) and jet width (h) and it is set to $15,000$. They used standard $k-\varepsilon$ turbulence model for the simulation of the turbulent offset jet. The physical geometry was considered same as [15, 27]. They concluded that the U_{max} and maximum value of wall shear stress decreases as the offset ratio increases. They also mentioned that the wall temperature is higher for $OR = 11$. Song et al. [28] studied the heat transfer and fluid flow characteristics of an inclined plane. They performed their experimental work by using liquid crystal to record the temperature for calculating the Nusselt number. Reynolds number was set to $53,200$ and the offset ratio was considered from 2.5 to 10. The oblique angle (α) was varied between $0^0 - 40^0$. They concluded that due to the turbulence mixing growth in the recirculation zone, the local Nusselt number increases in this region and found to be maximum in the reattachment point.

In the present modern era, some researchers [31, 32, 33, 34] also focused their attention in the fluid flow and heat transfer of three dimensional offset jet. Chaab and Tachie [34] used Particle Image Velocimetry (PIV) measurement technique in their experimental work and considered the three different Reynolds numbers (i.e., 5000, $10,000$, $20,000$). They also considered four offset ratios as 0.5, 1.0, 2.0, and 4.0. They investigated that the reattachment point is independent of the Reynolds number but depends upon the offset jet height. Assoudi et al. [33] studied the influence of density variation in the three dimensional offset jet. Three densities ($\rho_j = 1.25, 1.3, 1.4$) were considered for an offset height $h = 200mm$ along with three exit Reynolds numbers. They performed their experimental work with LDV technique and numerical analysis with RSM turbulence models. Mohmmadaliha [32] adopted the Yang-Shih low Reynolds number turbulence model to investigate the nozzle geometry for a $3D$ incompressible turbulent offset jet. They considered the three different nozzle geometries including circular nozzle, rectangular nozzle and square nozzle by keeping equal exit velocity. Circular nozzle and square nozzle were considered for the mean velocity characteristics and rectangular nozzle was considered to study the effect of aspect ratio. They concluded that the YS model is better than the other turbulence models for $3D$ but, for $2D$, high Reynolds number standard $k-\varepsilon$ model is better. Kashi et al. [35] did experiment and investigated the turbulence characteristics of the rectangular jet and compared this with the three-dimensional free jet and a wall jet. They used laser Doppler velocimetry technique for measuring the turbulence characteristics. They noticed that the crosswise distribution of Reynolds stress is same for both surface jet and a wall jet.

Going through the above mentioned literature it is realised that there are a dearth of literature on fluid flow and heat transfer characteristics of the offset jet. All the literature consdered only the plane wall surface~~Although, there are many literature on the offset jet~~, but almost little attention is paid on studying the fluid flow characteristics of a turbulent offset jet impinging on a wavy surface. In fact, to the authors' best knowledge there is no literature addressing this issue. However, it is well known that by increasing the surface area heat transfer increases drastically. The present study is aimed to bridge this gap in the literature. For this purpose, the waviness is created by using a sinusoidal function. The number of cycle is fixed to 10 while the amplitude is varied between 0.1 to 0.7 at an interval of 0.1. In the present study, the offset ratio (OR) is fixed to 7. Here, the definition of offset ratio ($OR = D/a$) is different than other definitions of offset ratio present in literature (see figure 1). A distinct fluid flow characteristic is observed owing to the presence of a wavy wall.

2 Governing equations and boundary conditions

In the computational domain, the flow is considered to be two-dimensional, steady state, turbulent and the fluid is assumed to be incompressible. To solve the physical behavior of turbulent flow, Finite Volume based Reynolds averaged Navier-Stokes (RANS) equations are incorporated. In the governing equation, body forces are neglected and the properties of the fluid are considered to be constant. The Reynolds stress are linked to the velocity gradient by using Boussinesq assumption. The Reynolds number is~~are~~ calculated based on the jet inlet velocity (U_0) and jet width (a) and set to $15,000$. ~~The computational domain is assumed to be fully turbulent.~~ The standard high Reynolds number two-equation $k-\varepsilon$ turbulence models is used. The non-dimensional parameters are used as described by Biswas and Eswaran [36] ~~are~~:

$$U_i = \frac{\bar{u_i}}{U_0}, \qquad X_i = \frac{\bar{x_i}}{a}, \qquad P = \frac{\bar{p} - \bar{p_0}}{\rho U_0^2}$$
$$k_n = \frac{k}{U_0^2}, \qquad \varepsilon_n = \frac{\varepsilon}{U_0^3/a}, \qquad \nu_{t,n} = \frac{\nu_t}{\nu} \tag{1}$$

Based on the above mentioned non-dimensionalized parameters, ~~T~~the non-dimensional governing equations are written in terms of indicial notation as:

Continuity equation:

$$\frac{\partial U_i}{\partial X_i} = 0 \tag{2}$$

Momentum equations:

$$\frac{\partial (U_j U_i)}{\partial X_j} = -\frac{\partial}{\partial X_i}\left(P + \frac{2}{3}k_n\right) + \frac{1}{Re}\frac{\partial}{\partial X_j}\left[(1+\nu_{t,n})\left(\frac{\partial U_i}{\partial X_j} + \frac{\partial U_j}{\partial X_i}\right)\right] \tag{3}$$

In above mentioned non-dimensional equations, k_n and $\nu_{t,n}$ represent~~show~~ the non-dimensional turbulent kinetic energy and the non-dimensional eddy viscosity, respectively. These equations are derived by adopting the concept of eddy viscosity. This equations for k_n and ε_n can be expressed as follows:

Turbulent transport equation $(\phi = k_n, \varepsilon_n)$:

$$\frac{\partial (U_j \phi)}{\partial X_j} = \frac{1}{Re}.\frac{\partial}{\partial X_j}\left[\left(1 + \frac{\nu_{t,n}}{\sigma}\right)\frac{\partial \phi}{\partial X_j}\right] + N_1 + N_2 \tag{4}$$

where σ, N_1 and $N_2 = \sigma_k$, G and $-\varepsilon_n$, respectively for k_n equation and σ_ε, $C_{1\varepsilon}\frac{\varepsilon_n}{k_n}G_n$ and $-C_{2\varepsilon}\frac{\varepsilon_n^2}{k_n}$, respectively for ε_n equation

Production (G_n) :

$$G_n = \frac{\nu_{t,n}}{Re}\left[\frac{\partial U_i}{\partial X_j} + \frac{\partial U_j}{\partial X_i}\right]\frac{\partial U_i}{\partial X_j} \tag{5}$$

Eddy viscosity ($\nu_{t,n}$):

$$\nu_{t,n} = C_\mu Re \frac{k_n^2}{\varepsilon_n} \tag{6}$$

The Launder and Spalding [17] proposed some empirical model constants for standard high-Reynolds-number two equations $k - \varepsilon$ model which are as follows: $\sigma_k = 1.0, \sigma_\varepsilon = 1.30, C_{1\varepsilon} = 1.44, C_{2\varepsilon} = 1.92$, and $C_\mu = 0.09$.

Non-dimensional boundary conditions are as follows:

Inlet of offset jet: $U = 1,\ V = 0,\ k_n = 1.5I^2,\ \varepsilon_n = k^{3/2}C_\mu^{3/4}/0.07$

Solid wall: $U = 0$ (no slip condition),$V = 0$ (no penetration condition), $k_n = 0,\ \varepsilon_n = 0$

Top boundary (entrainment side) : $\frac{\partial \phi}{\partial Y} = 0$, where $\phi = U_i,\ k_n$, and ε_n

Outflow boundary (exit side) : $\frac{\partial \phi}{\partial X} = 0$, where $\phi = U_i,\ k_n$, and ε_n

In the above mentioned boundary conditions, I represents the turbulent intensity which is considered to be 0.05. It is provided that near the solid wall, the first grid point should lie~~s~~ in the logarithmic region, i.e. $30 < Y^+ > 100$, where $Y^+ = \frac{yu_\tau}{v}$, u_τ is defined as the non-dimensional friction velocity.

3 Numerical Scheme

In the present work, the non-dimensional governing differential equations are discretised by using Finite Volume Method (FVM) on a collocated grid. To descretize the convective terms power-law upwind scheme is selected while for the diffusive terms, second order central difference scheme is considered. In order to couple the velocity and pressure, the semi-implicit method for pressure linked equation (SIMPLE) algorithm is considered which was proposed by ~~the patankar~~ Patankar [37]. Strongly Implicit Procedure (SIP) proposed by Stone [38] is used to solve the algebraic equations which comes after the discretization of the governing differential equations. The standard two equations $k - \epsilon$ turbulence model is considered to solve the 2-D Reynolds averaged Navier-Stokes (RANS) equations. It is noticed from the literature that this turbulence model provides better solution as compared to the low Reynolds number models like RNG $k-\varepsilon$ and Reynolds stress model (RSM) [39], Yang and Shih and Launder and Sharma turbulence models [40]. The domain size of $75a \times 60a$ is considered to implement the inflow and outflow boundary conditions in the X and Y directions respectively. Figures 2a and 2b show the layout of the domain size and the zoomed view of the grid near the wavy wall surface respectively.

4 Validation of code and grid independence test

In order to validate the developed code, the present result is validated with the experimental results of Song et al. [28] for the offset ratio 5 and the Reynolds number 53, 200. The graph has been plotted between $Y/Y_{0.5}$ and U/U_{max} for the three axial locations $X = 20$, 30, and 50 in figure 3. It is noticed that the present results provide the excellent agreement with the experimental results.

In the grid independence test, the three sets of non-uniform grid is considered with the collocated arrangement. The three grid densities of $202 \times 162\,(= 32724)$, $242 \times 192\,(46464)$ and $282 \times 222\,(62604)$ are considered and the results are compared for the offset ratio 7 and amplitude (A) 0.1 in figure 4. Figure 4a shows the decay of maximum streamwise velocity (U_{max}) in the axial direction and figure 4b describes the variation in the wall static pressure coefficient (C_{pw}) along the downstream direction for all three grid densities. From the figure 4, it is noticed that the grid sizes of 242×192 and 282×222 provide the more converged results. Thus, the grid size of 242×192 is considered for all the computational work.

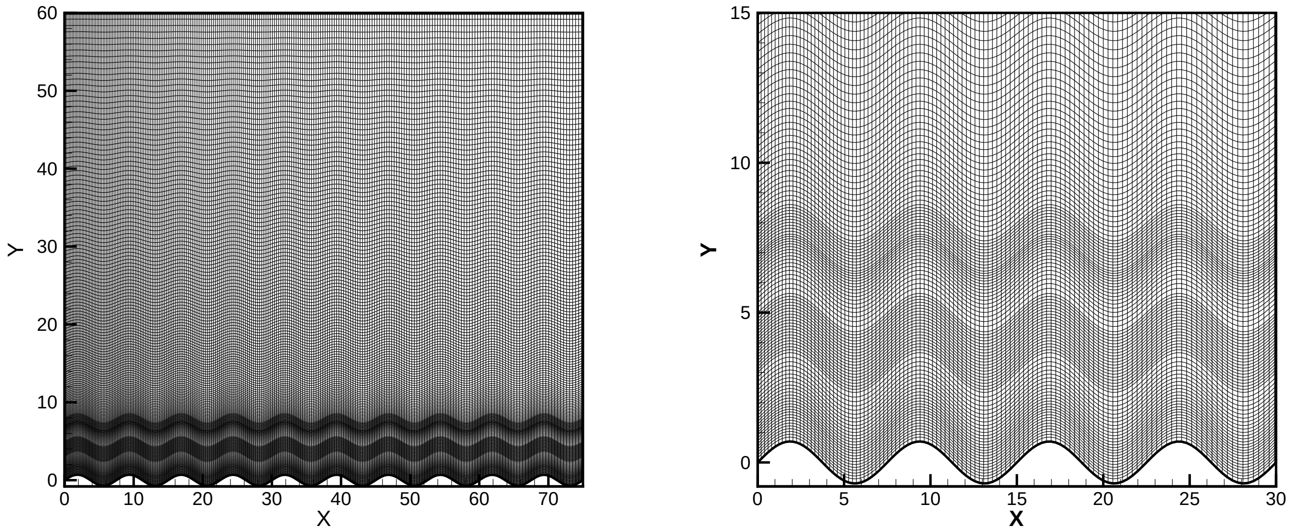

(a) Grid distribution of domain

(b) Grid distribution zoomed near the wavy wall

Figure 2: Typical grid distribution of dual jet flow domain

Table 1: Present result of various parameters for different amplitudes

A	X_{vc}	Y_{vc}	X_{rp}	P_{vc}	P_{min}	P_{max}	k_{max}	ϵ_{max}	$\lvert\overline{u'u'}\rvert_{max}$	$\lvert\overline{v'v'}\rvert_{max}$	$\lvert-\overline{u'v'}\rvert_{max}$
0.1	6.93	2.93	13.84	−0.094	−0.094	0.115	0.045	0.025	0.012	0.012	0.047
0.2	7.13	2.97	14.35	−0.089	−0.089	0.112	0.042	0.024	0.011	0.013	0.045
0.3	7.52	3.03	14.87	−0.083	−0.083	0.108	0.037	0.020	0.011	0.019	0.039
0.4	7.62	3.12	15.39	−0.083	−0.083	0.105	0.037	0.016	0.011	0.026	0.034
0.5	7.40	3.16	15.39	−0.080	−0.117	0.100	0.038	0.013	0.012	0.030	0.031
0.6	7.14	3.13	15.39	−0.085	−0.163	0.101	0.040	0.012	0.019	0.032	0.031
0.7	5.18	2.84	10.60	−0.143	−0.190	0.109	0.032	0.011	0.013	0.033	0.028

Table 2: Comparison list of various parameter of different author's

Various authors	OR	X_{vc}	Y_{vc}	X_{rp}	P_{min}	P_{max}	k_{max}	ϵ_{max}
Kumar [41, 42]	7.0	8.05	2.76	14.12	−0.085	0.107	0.048	0.039
Lund [4]	7.14	–	–	15.3	–	–	–	–
Rathore and Das [40], YS model	6.5	8.06	2.52	13.71	−0.059	0.09	–	–
Rathore and Das [40], LS model	6.5	8.20	2.49	13.76	−0.059	0.1	–	–
Rathore and Das [40], $k-\epsilon$ model	6.5	8.03	2.48	13.66	−0.059	0.1	–	–
Holland and Liburdy [27]	6.5	–	–	12.42	–	–	–	–
Vishnuvardhnarao and Das [26]	6.5	–	–	11.97	−0.04	0.2	–	–
Pelfrey and Liburdy [43]	6.5	7.0	2.5	13.00	–	–	–	–
Pramanik and Das [44] $\alpha = 10^0$	6.5	8.78	2.64	16.13	−0.064	0.07	0.050	0.065
Pramanik and Das [44] $\alpha = 0^0$	6.5	7.62	2.64	13.21	–	–	–	–
Correlation of Nasr and Lai [5]	6.5	–	–	13.78	–	–	–	–

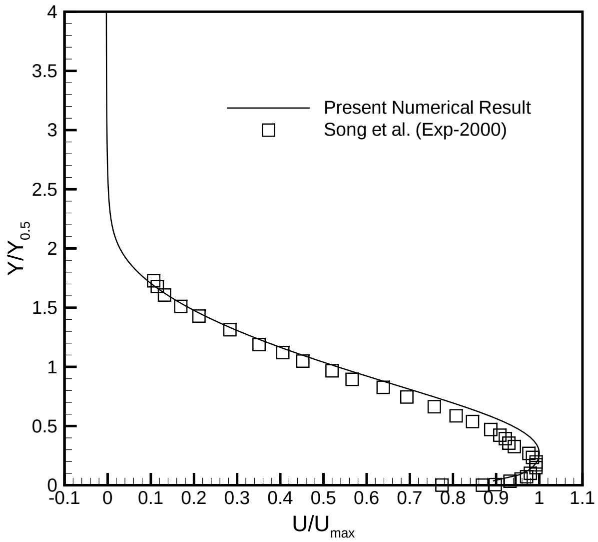

(a) X=20

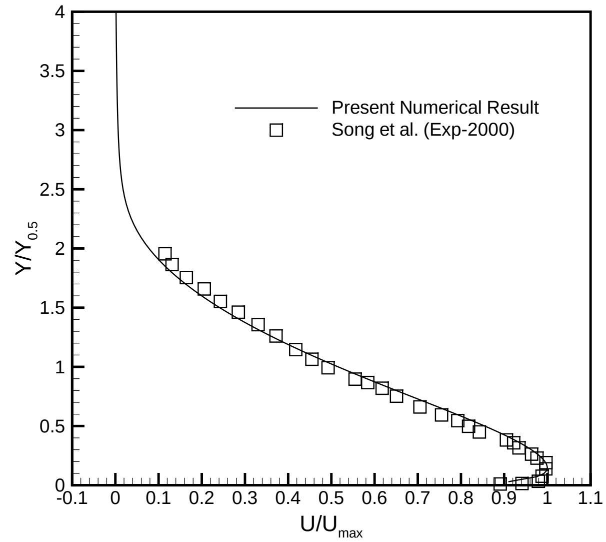

(b) X=30

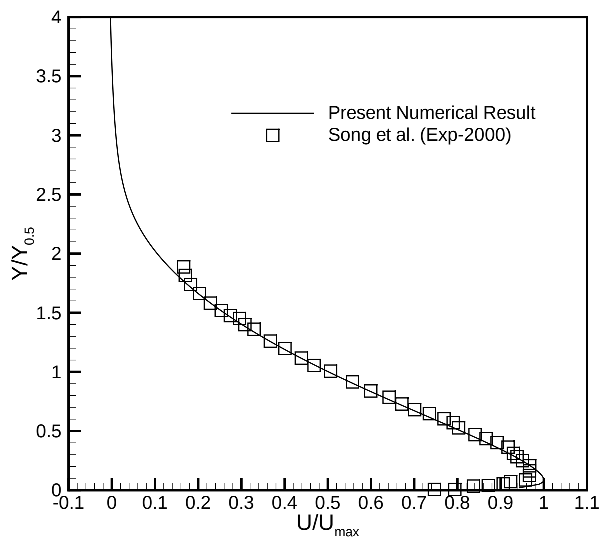

(c) X=50

Figure 3: Code validation for OR=5 with experimental results of Song et al. [28]

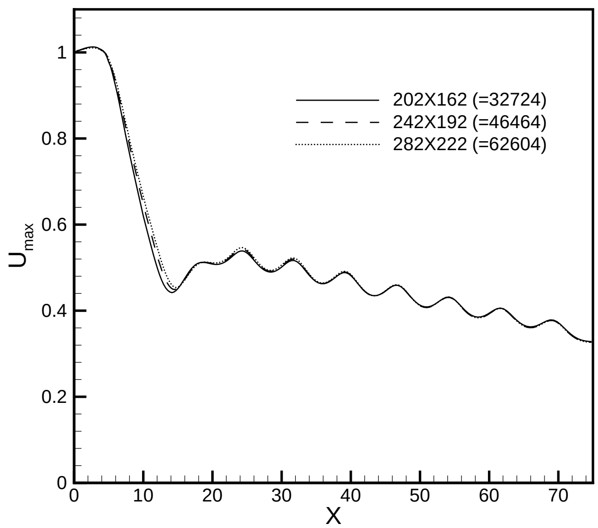

(a) Decay in maximum streamwise velocity (U_{max}) along the X- direction

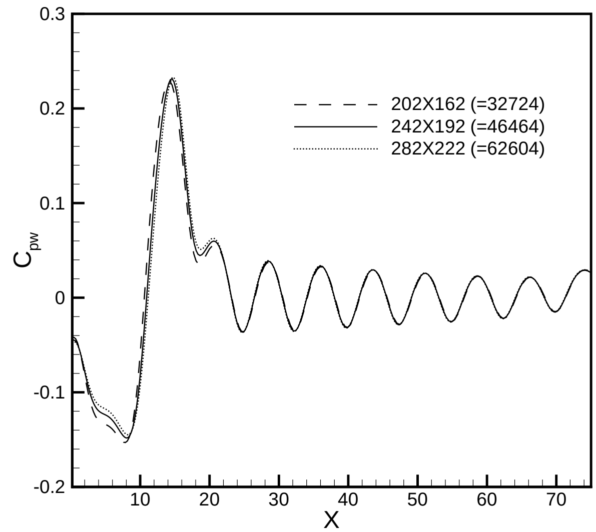

(b) Variation of wall static pressure coefficient (C_{pw})

Figure 4: Results of grid independence study for $OR = 7$ at $A = 0.1$

Table 3: Comparison of the values of Reynolds stresses of different authors

Various authors	$\lvert\overline{u'u'}\rvert_{max}$	$\lvert\overline{v'v'}\rvert_{max}$	$\lvert-\overline{u'v'}\rvert_{max}$
Kumar [42]	0.031	0.036	0.018
Rathore and Das [40], YS model	–	–	0.01
Rathore and Das [40], LS model	–	–	0.01
Rathore and Das [40], $k-\epsilon$ model	–	–	0.01
Pramanik and Das [44] $\alpha = 10^0$	0.03	0.040	0.017

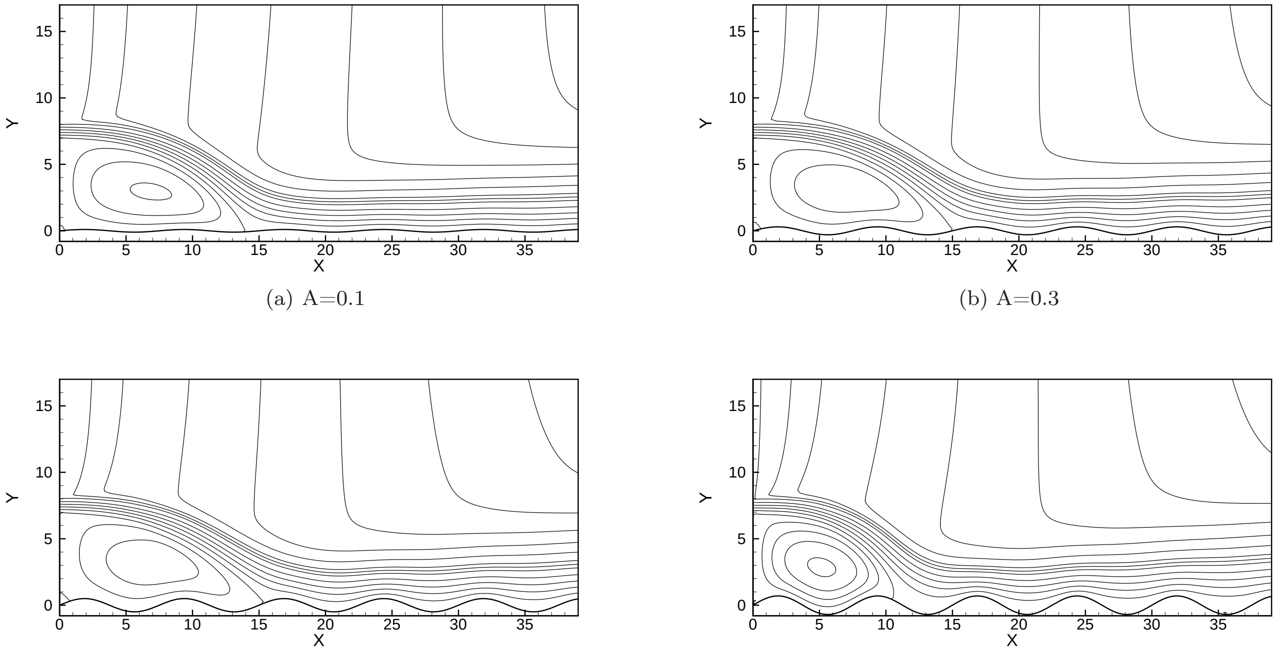

(a) A=0.1

(b) A=0.3

(c) A=0.5

(d) A=0.7

Figure 5: Streamline contours for various amplitudes

5 Results and discussion

The present computational results are presented for the offset jet with an offset ratio equal to 7. The wall is wavy in nature with the varying amplitudes. The amplitude of the wavy surface is varied from 0.1 to 0.7 with an interval of 0.1. The number of cycle for all the computations is set to 10. The Reynolds number is considered to be $15,000$ to make the inlet condition ~~present flow domain~~ fully turbulent. The fluid flow and turbulent characteristics are presented in the form of contours and tabular form. The definition of the OR in present numerical work is the ratio of the offset distance from the wall to the bottom of the jet (D) to the jet width (a). The definition of the OR is different from the definition of OR present in the literature [26, 40, 6, 27, 44].

5.1 Streamlines and velocity vector contours

In order to study the flow characteristics of the fluid flow, the streamline and the velocity vector plots for the different amplitudes are presented in the figure 5 and figure 6. The streamlines of the various amplitudes are plotted in figure (5a-5d). ~~When the fluid is discharged from the jet, the pressure difference occurs across the jet. The low atmospheric pressure region is created between the jet exit and the wall below the jet, and due to this low pressure zone, the issuing jet tilt towards the plate and strikes the plate, this is because of the "Coanda effect"[11]. The low sub-atmospheric pressure region is known as the recirculation region and the point at which the inner shear layer of the jet attaches to the wall is termed as the reattachment point.~~ The formation of the vortex centers in the recirculation region may be seen easily (see figure 5a-5d). In the present study the amplitude of the wavy surface ~~with varied amplitude~~ is varied~~used~~. From the figure 5, it can be seen that the position of the vortex center changes as the amplitude of the wavy surface increases. The value of the vortex centers for all the values of the amplitude~~s~~ from 0.1 to 0.7 is presented in table 1. It is noted that as the amplitude increases, the X_{vc} and Y_{vc} increase and at $A = 0.4$ and $A = 0.5$, maximum value of the X_{vc} and Y_{vc} is found respectively. After that, X_{vc} decreases as the amplitude increases from $A = 0.4$ to $A = 0.7$ so as the Y_{vc} from $A = 0.6 - 0.7$. The reason is quite obvious that the minimum pressure in the recirculation region increases with increase in the amplitude beyond 0.4. This attracts the jet more

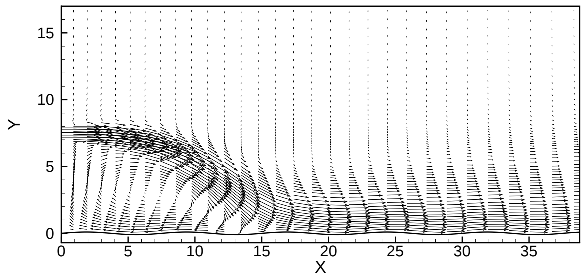

(a) A=0.1

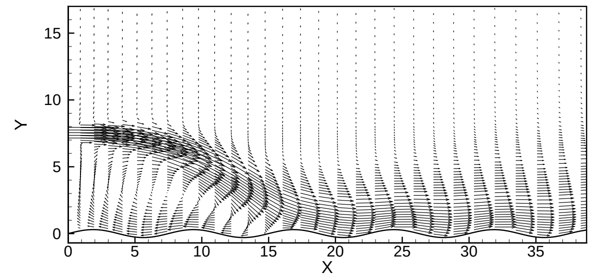

(b) A=0.3

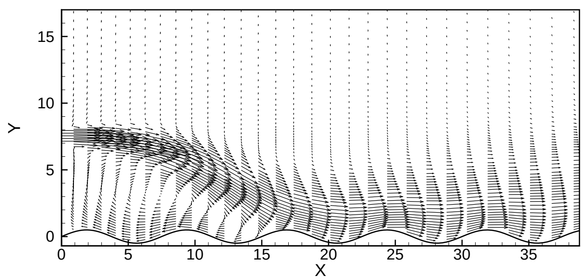

(c) A=0.5

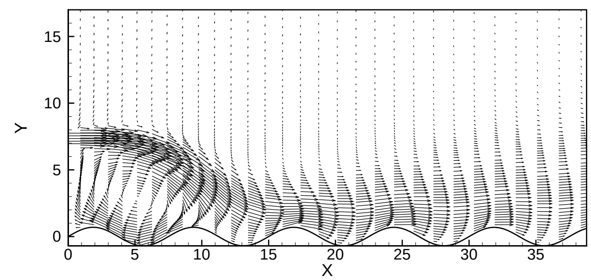

(d) A=0.7

Figure 6: Velocity vector contours for various amplitudes

towards the wall; as a result, X_{vc} and Y_{vc} decrease.~~The reason might be possible that the magnitude of P_{min} of domain decreases rapidly when amplitude increases beyond 0.4, which might have forced the position of X_{vc} and Y_{vc} to move toward the nozzle and close to the plate.~~ For the comparison purpose, the value of vortex center obtained by the different researchers are also presented in table 2. The present result~~s~~ of X_{vc} is higher than~~from~~ the experimental results of Pelfrey and Liburdy [6], but is~~has the~~ lower than the values ~~as~~ compared with~~from~~ the other numerical results (see table 2).

The velocity vector plots for the different values of the amplitude are shown in the figure 6. Figures 6a-6d show~~s~~ the variation of the mean velocity vector for each of the amplitude very clearly. The size of the recirculation region increases up to $A = 0.6$. But for the $A = 0.7$, the size of the recirculation region is lower. After the reattachment point (X_{rp}), the flow develops along the wavy surface. ~~The pressure in the recirculation region plays a big roll here. When, $A = 0.7$ the P_{min} is very low and enhance the strength of recirculation region which force the jet to attract the surface so early. This might be one of the reason why X_{rp} is low when $A = 0.7$.~~ The reattachment point (X_{rp}) for the various amplitudes is presented in table 1. It is found that as the amplitude of the wavy surface increases, the reattachment point increases up to $A = 0.6$. It is noted that the the value of X_{rp} for other researcher are less accept the Pramanik and Das [44], because they have used the inclined plate having oblique angle 10^0.

5.2 Pressure contour

Figure 7 represents the pressure contour in the computational domain. In the figure 7, the dotted lines represent the low ~~sub~~-atmospheric pressure. The formation of the recirculation region is due to the presence of the low atmospheric pressure between the ~~exit~~ jet and the ~~presence of the~~ wall which makes the jet to attract~~deflect~~ towards the wall. For the offset jet with $OR = 6.5$ having plane wall surface, the P_{min} lies in the recirculation region at the vortex centre [26, 6]. But, for the wavy surface some interesting facts have been observed. To mention the present observation, the pressure in the low ~~sub~~-atmospheric region are divided into P_{vc} and P_{min}. In ~~the~~ table 1, the minimum pressure at the vortex centre (P_{vc}) and the minimum pressure (P_{min}) in the low~~sub~~-atmospheric region~~domain~~ for various amplitudes are listed. It is noticed that

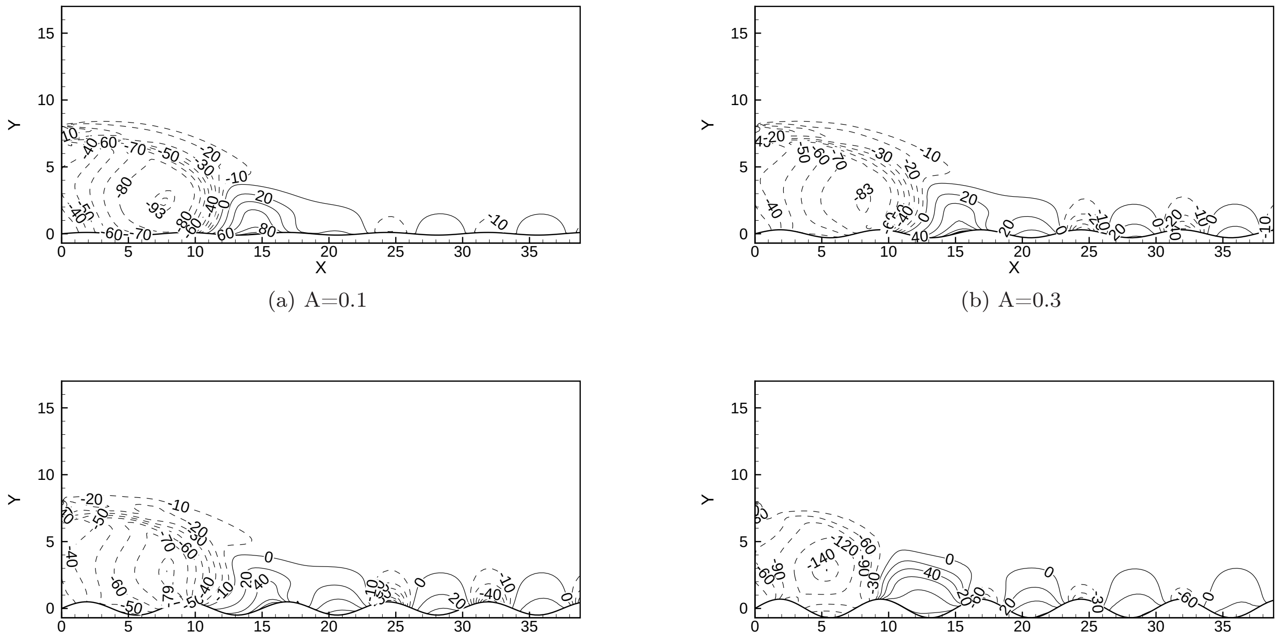

(a) A=0.1 (b) A=0.3

(c) A=0.5 (d) A=0.7

Figure 7: Pressure ($\times 10^3$) contours for various amplitudes

the minimum pressure at the vortex center (P_{vc}) and the minimum pressure (P_{min}) in the recirculation region are same and increase~~s~~ as the amplitude of the wavy surface increases upto $A = 0.4$. After that, these two differ significantly ~~As the amplitude of the wavy surface increases beyondbeyound 0.4, the values of P_{vc} and P_{min} differ~~ (refer table 1). The pressure at the vortex centre increases for $A = 0.5$ and then suddenly decreases for $A = 0.6$ and $A = 0.7$. It is noticed that for amplitudes $A \geq 0.5$, the P_{min} decreases very sharply and this value of P_{min} for amplitudes 0.5, 0.6, and 0.7 is noticed near the nozzle. Also, in the recirculation region, the pressure decreases sharply with increase in the amplitude of wavy surface beyond A=0.4. Due to this combined effect, the jet deflects even more towards the wall so early for A=0.7 (see figure 7a-7d). The maximum value of pressure (P_{max}) is observed to be near the reattachment point and decreases as the amplitude of the wavy surface increases but, for $A = 0.7$, P_{max} is found to be greater than the value of $A < 0.3$. For comparison purpose, the values of P_{min} and P_{max} of different authors are mentioned in the table 2 for the plane wall surface. The minimum value of the pressure is noticed at the vortex center in the recirculation region and the maximum value of the pressure is noticed near the reattachment point. From figures 7a-7d, it is observed that the minimum value of the pressure (P_{min}) in the recirculation region and the maximum value of the pressure (P_{max}) near the reattachment point decrease as the amplitude of the wavy wall surface increases. The value of P_{min} decreases in the recirculation region as the amplitude increases which indicates that the strength of that zone also increases simultaneously. The value of P_{min} and P_{max} are mentioned in ~~the~~ table 1 for the various amplitudes. It is observed that when the wavy wall is used, the value of P_{min} decreases as compared to the plane wall for the same offset ratio (please refer table 2).

5.3 k_n and ε_n contour

Figure 8 and figure 9 represent the variation~~flow field~~ of the non-dimensional turbulent kinetic energy and the rate of dissipation for the variou~~sed~~ amplitudes of the sinusoidal wavy surface. Turbulence kinetic energy (k_n) is the energy content of the eddies in turbulent flows; larger the size, the higher is energy content of eddies. From figure 8, it is noticed that the value of the maximum turbulent kinetic energy is found to be near~~at~~ the exit of the jet, because ~~at that time~~ the ~~fluid of the exit~~ jet interacts with the surrounding

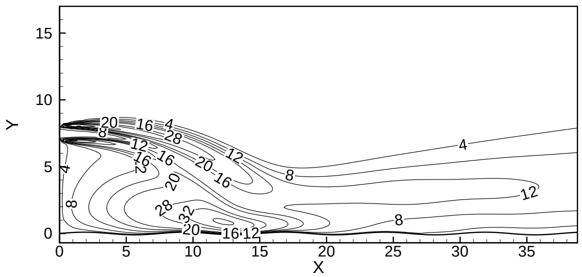

(a) A=0.1

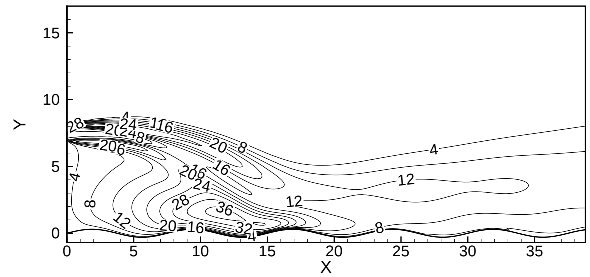

(b) A=0.3

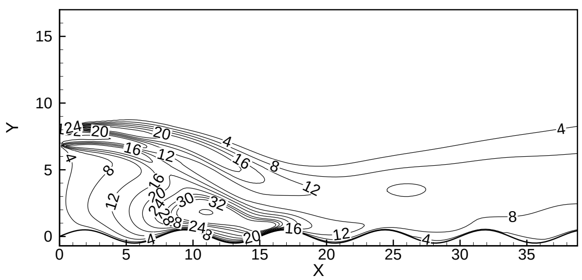

(c) A=0.5

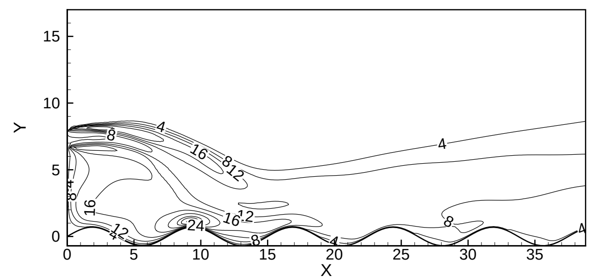

(d) A=0.7

Figure 8: Turbulent kinetic energy ($k_n \times 10^3$) contours for various amplitudes

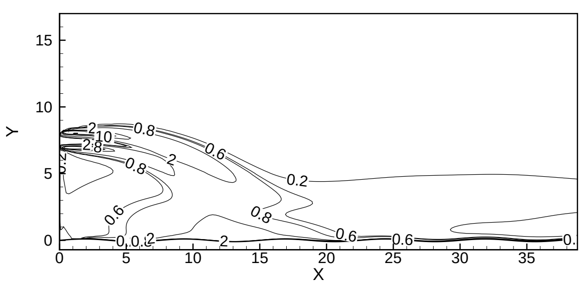

(a) A=0.1

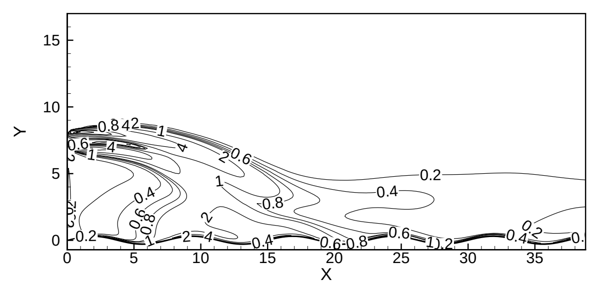

(b) A=0.3

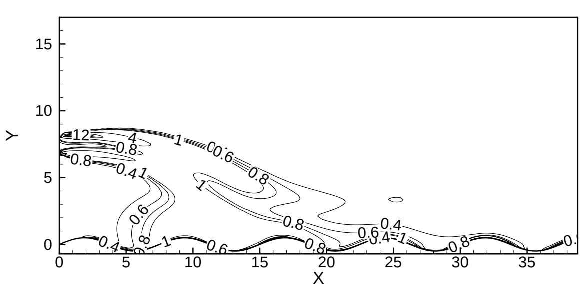

(c) A=0.5

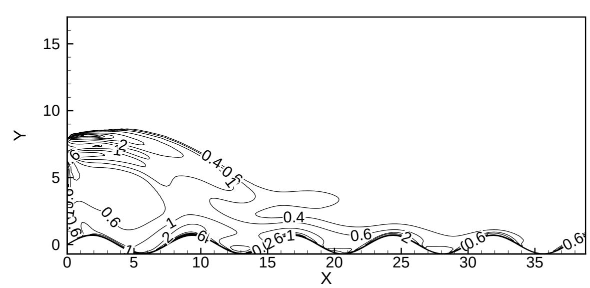

(d) A=0.7

Figure 9: Dissipation rate ($\varepsilon_n \times 10^3$) contours for various amplitudes

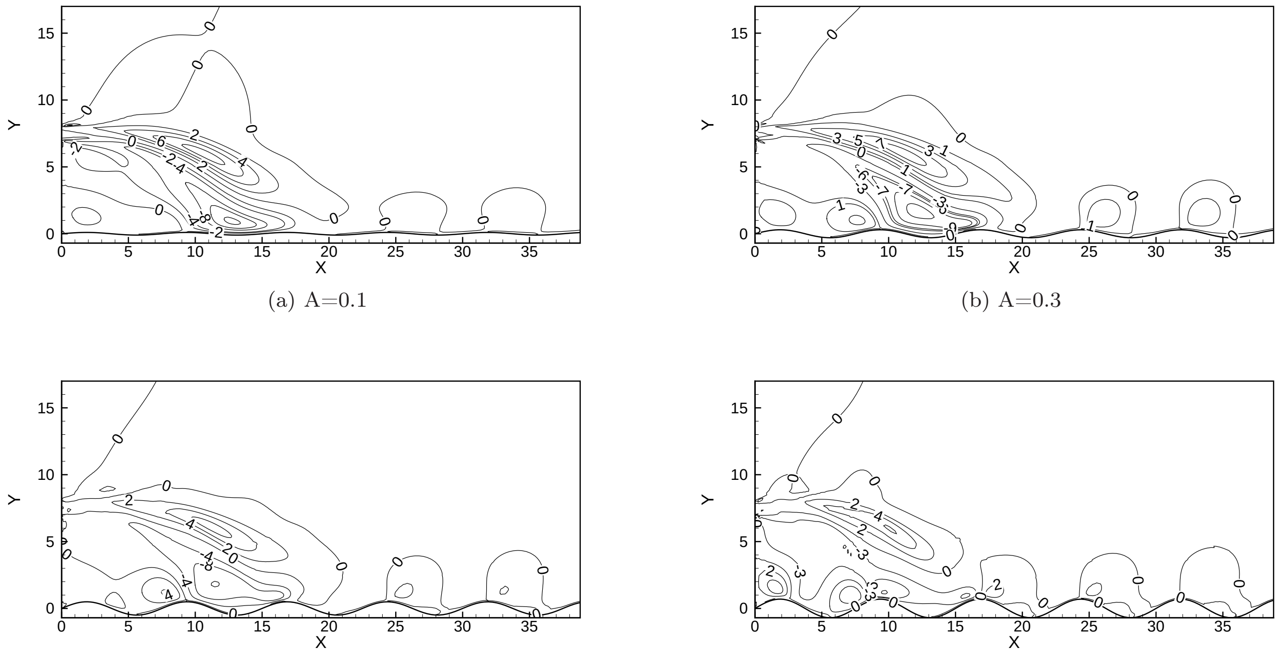

(a) A=0.1

(b) A=0.3

(c) A=0.5

(d) A=0.7

Figure 10: Contours of normal Reynolds stress along X-axis ($\overline{u'u'} \times 10^3$) for various amplitudes

quiescent fluid. ~~when $A = 0.3$.~~ As compared to all three regions of the offset jet, the higher value of k_n lies in the recirculation region when A increases beyond 0.3 than the other two regions. It suggests that increase in the amplitude of the wavy surface reduces the size of the eddies which causes the decrease in the value of k_{max}. Table 1 lists that as the amplitude increases, the k_n decreases and then increases. From figures 8a-8d, it is seen that the minimum value of k_{max} is noted for the maximum value of the amplitude 0.7 in the recirculation region. When compared to the other plane wall results, it is noticed that k_{max} decreases with the increase in the amplitude of the wavy wall (see table 2).

The distribution of non-dimensional dissipation rate (ϵ_n) is shown in figure 9 for the various amplitudes. In the offset jet, the maximum energy is dissipated near the jet exit. The minimum value of ε_n is noticed in the recirculation ~~recirculation~~ region and it decreases continuously along the flow direction. Kumar [42] calculated the maximum value of dissipation rate (ε_{max}) of an offset jet ($OR = 7.0$) for the plane wall as 0.039. While Pramanik and Das [44] noticed the maximum value of ε_{max} of offset jet ($OR = 6.5$) for inclined plane wall as 0.065. When the wavy surface is used, it is found that the value of ε_{max} is located above the nozzle and it ~~is~~ decreases ~~noticed that~~ as the amplitude of the wavy surface increases ~~the the value of ε_{max} decreases~~. (please refer table 1). The reason might be that as the amplitude of sinusoidal wavy surface increases the energy is dissipated from large vortices to small vortices very fast. The minimum value for ε_{max} is noted as 0.011 for the higher amplitude 0.7.

5.4 Reynolds shear stress contour

The non-dimensional Reynolds stress $\overline{u'u'}$, $\overline{v'v'}$ and $\overline{-u'v'}$ contour plots for the various amplitudes are shown in figures 10, 11 and 12 respectively. The magnitude of normal Reynolds stress along $x-$direction $\overline{u'u'}$ is found to be maximum when the amplitude is 0.6 (see table 1) but the magnitude of $\overline{v'v'}$ increases as the amplitude of the wavy surface increases from 0.1 to 0.7 (see table 1). The magnitudes of $\overline{u'u'}$ and $\overline{v'v'}$ are higher in the recirculation region due to the vigorous turbulence which is present in this region. The distribution of Reynolds stress $-\overline{u'v'}$ ~~$(-\overline{u'v'})$~~ for the different amplitudes are shown in figure 12. The dotted line in the contours are for the negative values. The maximum value of the $|-\overline{u'v'}|$ are found to be near the

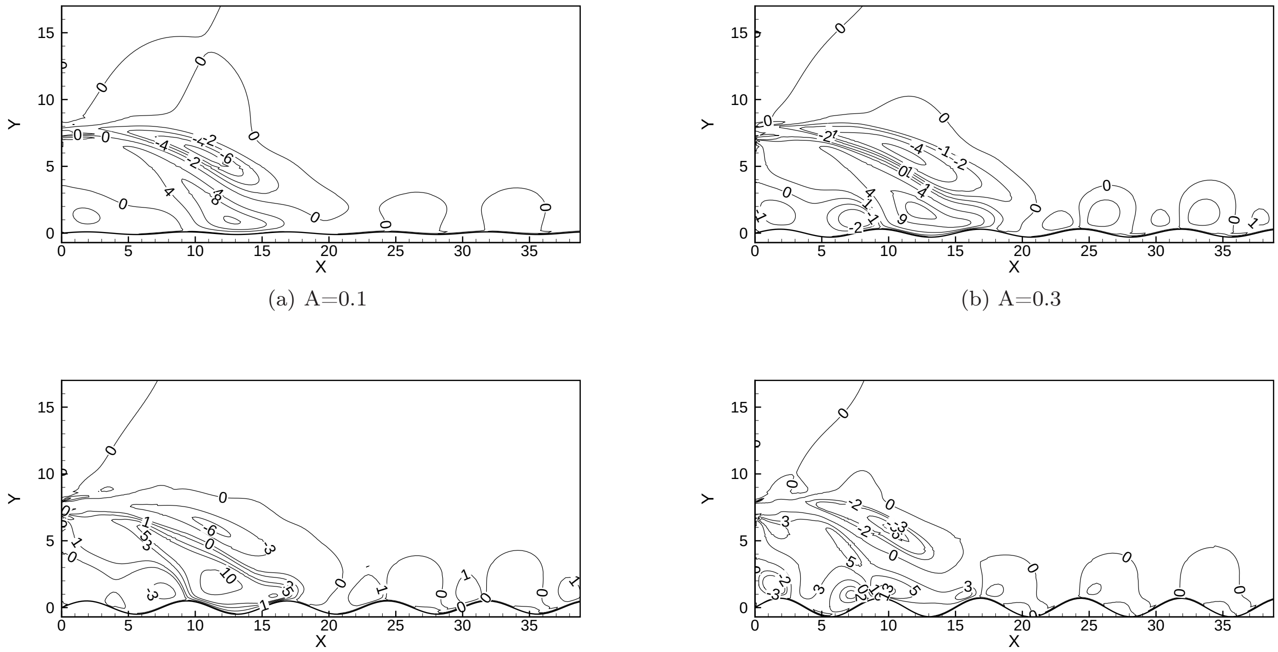

(a) A=0.1 (b) A=0.3 (c) A=0.5 (d) A=0.7

Figure 11: Contours of normal Reynolds stress along Y-axis ($\overline{v'v'} \times 10^3$) for various amplitudes

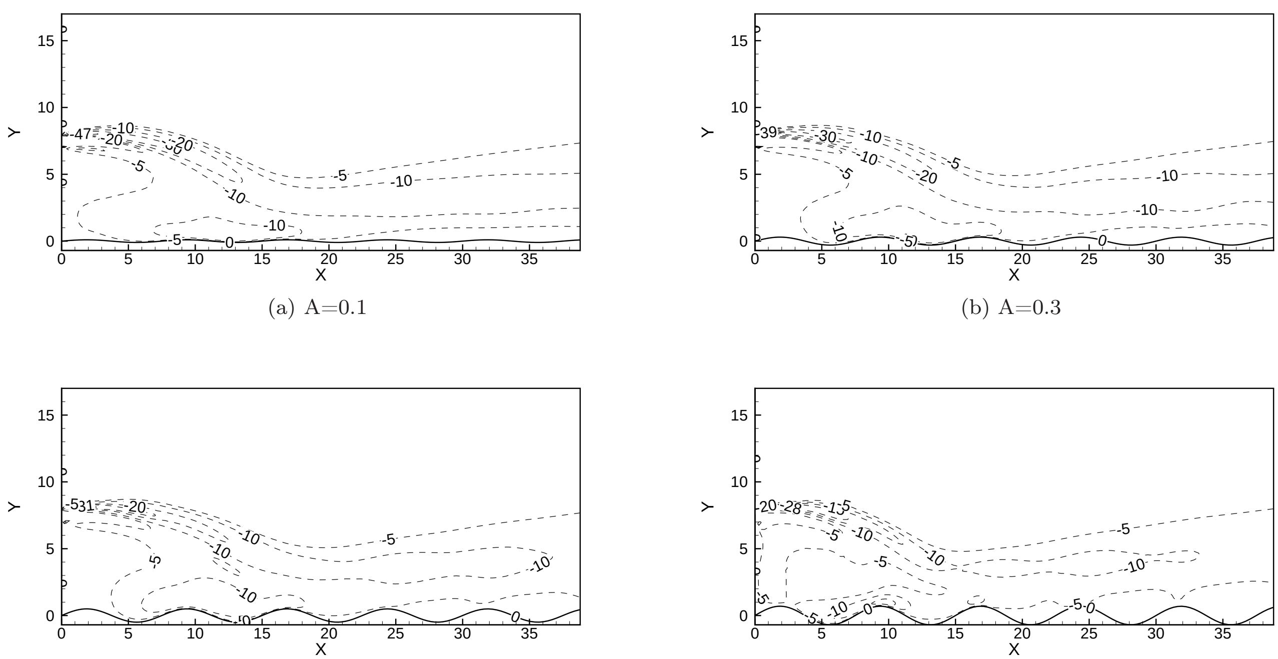

(a) A=0.1 (b) A=0.3 (c) A=0.5 (d) A=0.7

Figure 12: Contours of Reynolds stress ($-\overline{u'v'} \times 10^3$) for various amplitudes

Table 4: Value of total momentum flux (F_{total}) for various amplitudes

A	0.1	0.2	0.3	0.4	0.5	0.6	0.7
F_{total}	0.735	0.722	0.705	0.686	0.662	0.699	0.609

Table 5: Comparison of total momentum flux for various authors

Kumar [41]	Rathore and Das [40] $OR = 6.5$			Pramanik and Das [44]
$OR = 7.0$	YS model	Standard $k-\varepsilon$ model	LS model	$OR = 6.5,\ \alpha = 10^0$
0.744	0.808	0.764	0.815	0.8

reattachment ~~reattechment~~ point because, at this point, the jet tries to attach to the wall. The maximum value of the $|-\overline{u'v'}|$ decreases as the amplitude of the wavy wall surface increases (see table 1).

5.5 Momentum flux

The momentum flux of the offset jet for various amplitudes of the wavy wall surface is shown in figure 13. To calculate the momentum flux, the $X-$momentum equation is integrated over the defined computational domain. The results of this integration comes in the form of integral constant: $F_{total} = \int_{Y_{min}}^{Y_{max}} (F_u + F_p + F_k + F_r)dY =$constant. The Boussinesq model (i.e. $\overline{u'u'} = \frac{2}{3}k_n - \frac{2}{Re_t}\frac{\partial U}{\partial X}$) is used to compute the Reynolds stress. The individual terms are computed as $F_u = \int UUdY$, $F_p = \int PdY$, $F_k = \int (2/3)k_n dY$ and $F_r = -\int (2/Re_t)(\partial U/\partial X)dY$, and compared for the different amplitudes of the wavy surface. Figure 13 presents the F_u, F_p, F_k, F_r and $F_{total} = (F_u + F_p + F_k + F_r)$ for the amplitude of $A = 0.1$, 0.3, 0.5 and 0.7. The individual terms F_u, F_p, F_k, F_r and F_{total} are presented in the form of the different symbols notation. From figure 13a to figure 13d, it can be seen that the momentum flux is mainly influenced by the F_u and F_p and they show the opposite trend in the recirculation and impingement regions. The other two terms, F_k and F_r, are not so dominant in the momentum flux because they have very small values. The momentum flux by the pressure F_p decreases in the recirculation region and then increases up to the reattachment point. After that it decreases and follow the wavy pattern in the flow direction. The decrease of F_p after the reattachment point is because of the pressure head changeover the velocity head. The F_u shows the opposite trend from F_p. After the exit of the nozzle, the F_u increases and attains the maximum value and then decreases and attains the minimum value near the reattachment point. The F_u, then recovers and follows the wavy pattern in the wall jet region. The F_u decreases in the wall jet region as the amplitude increases. It is mainly because of frictional resistance provided by the wavy wall. It should be noted here that the F_u is maximum where F_p is minimum and vice-versa. The value of F_{total} in the wall jet region decreases very slowly and remains almost constant. The value of integral constant (F_{total}) in the wall region decreases as the amplitude of the wavy surface increases up to the amplitude 0.5. There after, for the amplitude 0.6, F_{total} increases and, then again decreases and attains the minimum value for the higher amplitude 0.7. (see table 4). For comparison purpose, the integral constant for the various researchers [41, 40, 44] is also listed in the table 5.

Figure 14 is presented to notice the variation in F_u and F_p for the various amplitudes. For the comparison purpose, the results of other authors are also plotted along with the present numerical results. It can be observed from the figure 14a that when the amplitude is higher (i.e. $A = 0.7$), the value of F_u is higher in the recirculation region as compared to other amplitude and low Reynolds number models for the plane wall of Rathore and Das [40]. In the impingement region, a small amount of increment is found in the value of F_u. The value of F_u then slightly decreases in the wall jet region, but the decrease in the value of F_u increases as the amplitude of the wavy surface increases as compared to the LS model, YS model and the $k-\varepsilon$ model of the plane wall surface of Rathore and Das [40] and follows the wavy pattern afterwards. Figure 14b also indicates that after the exit of nozzle, the value of F_p decreases more in the recirculation region and attains the minimum value at the higher amplitude of the wavy wall surface (i.e. $A = 0.7$). The value of F_p then increases in the recirculation region and attains the maximum value near the reattachment point for the higher amplitude of the wavy surface as compared to others results [44, 40], then decreases in

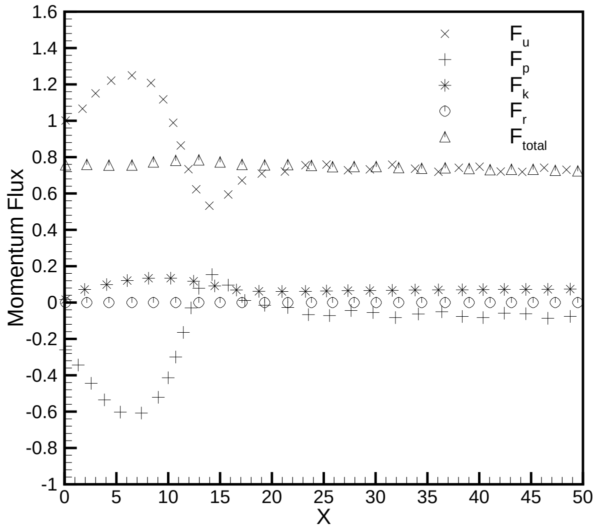

(a) A=0.1

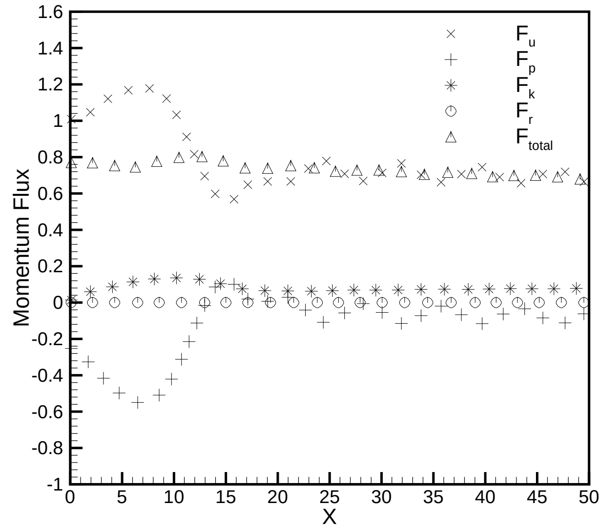

(b) A=0.3

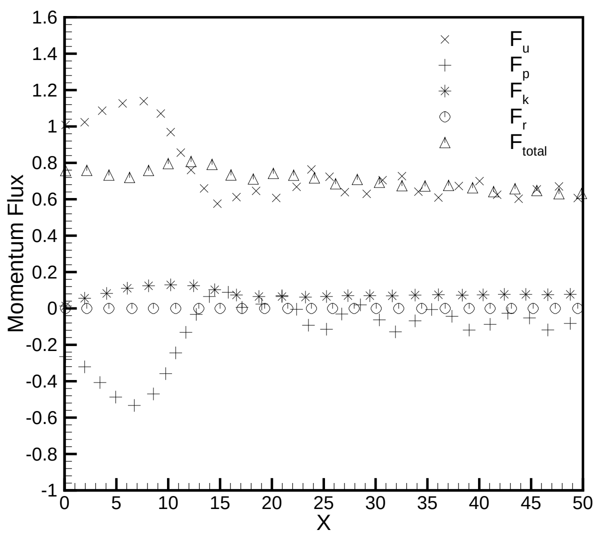

(c) A=0.5

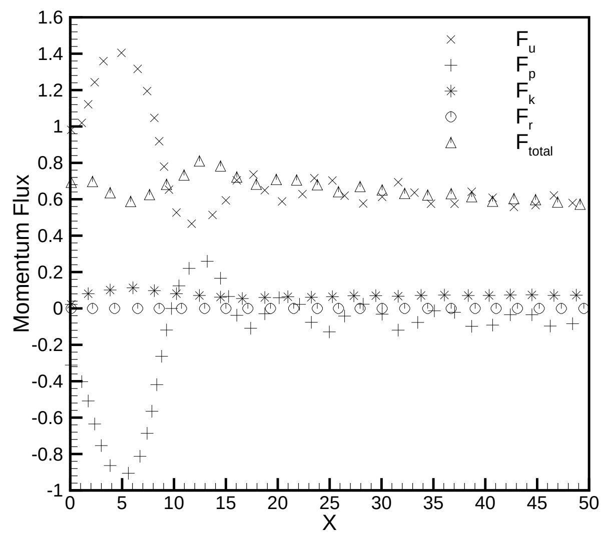

(d) A=0.7

Figure 13: Momentum flux term by term for various amplitudes

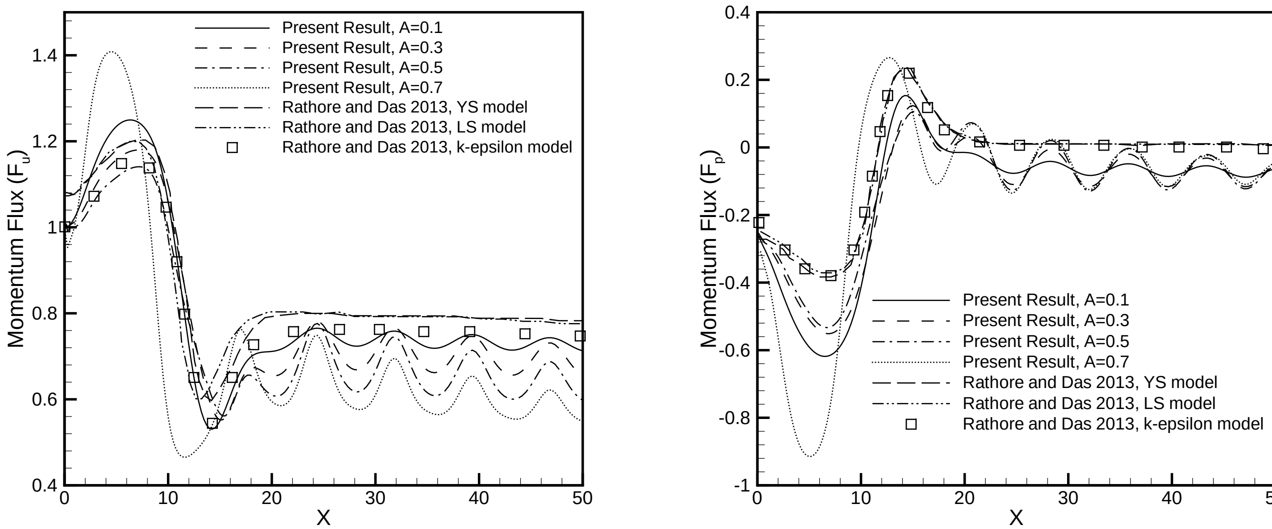

(a) Comparison of F_u momentum flux along $X-$direction

(b) Comparison of F_p momentum flux along the flow

Figure 14: Comparison of F_u and F_p Momentum fluxes

the impingement region and wall jet region for the all the amplitude of the wavy surface followed by wavy pattern~~lattern~~. The value of F_p remains almost constant for the plane wall of Rathore and Das [40] with low Reynolds models and inclined plane wall of Pramanik and Das [44].

5.6 Similarity solution

The flow characteristics of an offset jet attain the flow characteristics of a wall jet in the wall region. To find out the velocity similarity profile in this region, Wygnanski et al. [45] came up with the concept of traditional outer scaling method where the curve is plotted between U/U_{max} and $Y/Y_{0.5}$. The $Y_{0.5}$ denotes the non-dimensional position in the cross-stream direction where $U = U_{max}/2$. To resolve the variation in the wall region, the scaling of crosswise direction in the plot has been done by Y_1 which denotes the first grid position on the surface at the crest and at the trough. To demonstrate the scaled velocity similarity profile for the present wavy surface, four axial locations of the crest (i.e., 31.91, 39.35, 46.97, and 54.34,) and trough (i.e., 35.73, 43.10, 50.60, and 58.19) in the wall region for the amplitudes 0.1, 0.4 and 0.7 are presented in the figure 15. It can be noticed that for all the cases similarity solution is achieved with a little deviation in the outer region characterised as $\frac{Y-Y_1}{Y_{0.5}-Y_1} \geq 1.0$. Even though similarity solution is achieved for all the cases but the trend is entirely different than the case of a plane wall (Kumar [41, 42, 46]). The similarity solution at the crest is different than at the trough. Moreover, the similarity solution is even different for the case of A=0.7 (see figures 15e and 15f).

The velocity self-similarity solution for different amplitudes is compared at a fixed position of crest and trough in the wall region in the figure 16. The profile for crest and trough is considered at $X = 54.34$ and $X = 58.19$ respectively. Figure 16a shows that at a crest position of $X = 54.34$ near the wall region, all the lines collapsed into one. It is also observed that when $\frac{Y-Y_1}{Y_{0.5}-Y_1} \geq 0.1$ the deviation of the profiles for $A = 0.5$ and $A = 0.7$ are more whereas, when $\frac{Y-Y_1}{Y_{0.5}-Y_1} \geq 1.1$ the deviation in the outer region is small for $A = 0.7$. Further, it is also seen that the velocity profile for $A = 0.1$ and $A = 0.3$ is almost similar. Figure 16b represents the distribution of self-similarity at a trough position of $X = 58.19$ in the wall region. From figure 16b it is seen that when $\frac{Y-Y_1}{Y_{0.5}-Y_1} \leq 1.0$, the deviation of the profile for the different amplitudes is very high. However, for outer region (i.e., $\frac{Y-Y_1}{Y_{0.5}-Y_1} \geq 1.0$) little deviation is noticed. Also, it can be seen that as the amplitude of the wavy surface increases the inflection point in the profile moves in the crosswise~~-stream~~

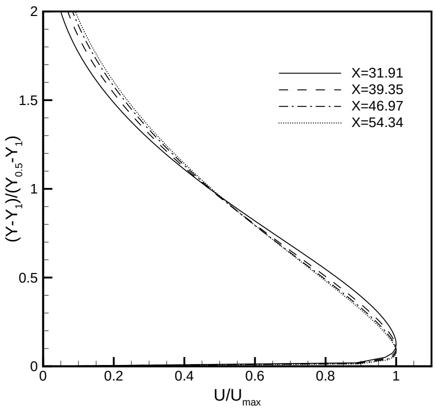

(a) Similarity solution at crest for $A = 0.1$

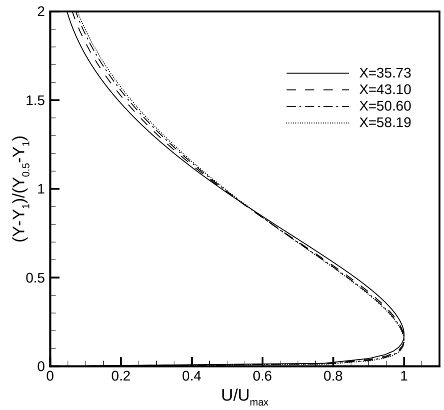

(b) Similarity solution at trough for $A = 0.1$

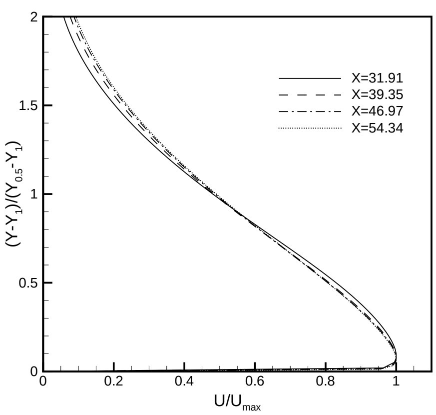

(c) Similarity solution at crest for $A = 0.4$

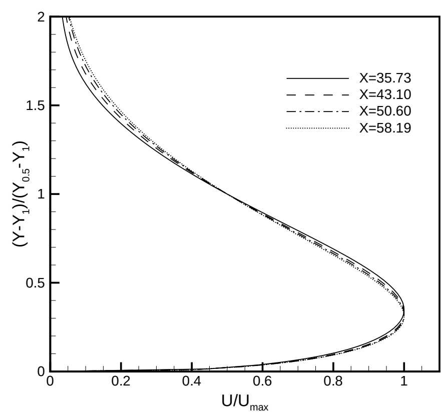

(d) Similarity solution at trough for $A = 0.4$

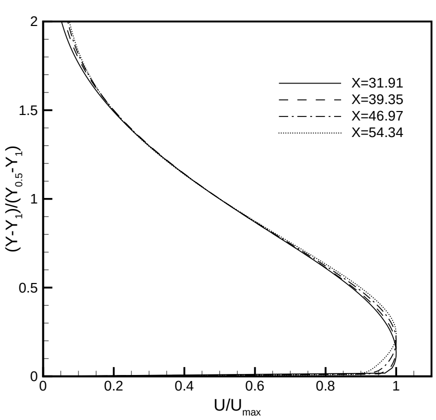

(e) Similarity solution at crest for $A = 0.7$

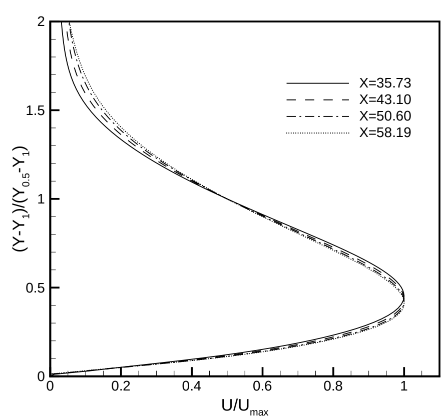

(f) Similarity solution at trough for $A = 0.7$

Figure 15: Similarity solution comparison for crest and trough for $A = 0.1$, 0.4, and 0.7 in four downstream locations

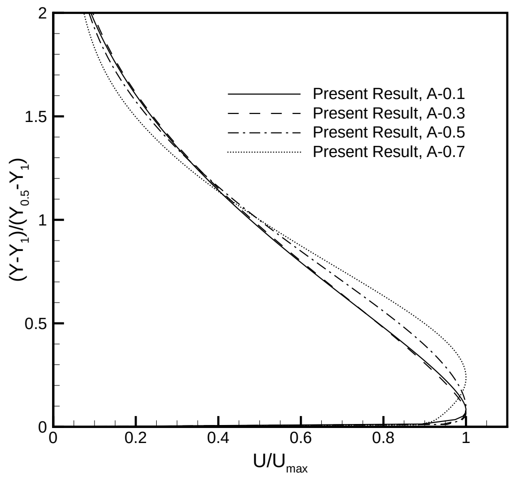

(a) Similarity solution comparison for various amplitudes at crest position $X = 54.34$ in wall region

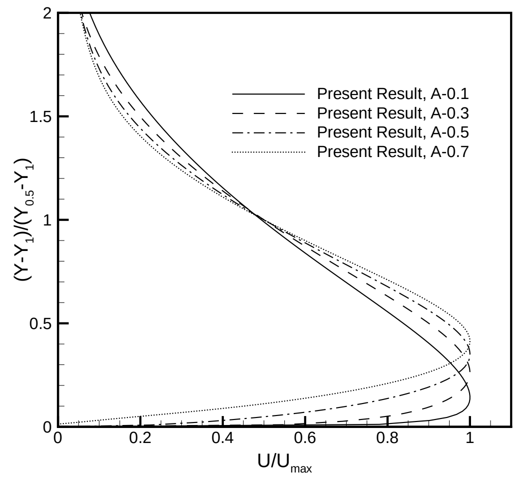

(b) Similarity solution comparison for various amplitudes at trough position $X = 58.19$ in wall region

Figure 16: Similarity solution for different amplitudes 0.1, 0.3, 0.5, and 0.7 at fixed crest and trough position in downstream direction

direction.

5.7 Distribution of wall shear stress

In order to show the distribution of the wall shear stress along the wall, figure 17 is presented. The present results of wavy surface with various amplitudes are plotted along with the plane wall surface of Vishnuvardhanarao and Das [26]. It is noticed that the value of the wall shear stress increases gradually for the plane wall surface of Vishnuvardhanarao and Das [26], but for all of the values of amplitude, it increases slowly, and then decreases but, again increases in the recirculaton region. The value of wall shear stress is positive in the recirculation region. It can be seen from figure 17 that the maximum value of wall shear stress increases as the amplitude increases and attains the maximum value for the higher amplitude $A = 0.7$. The wall shear stress becomes equal to zero at the reattachment point. The value of wall shear stress decreases continuously in the impingement region. The wall shear stresses for the plane wall [26] increases gradually in the wall jet region where as wall shear stress for all the amplitude again increases suddenly and follow the wavy pattern in wall jet region. The fluctuation of wall shear stress is more near the beginning of wall jet region as the amplitude increases because the higher value of amplitude provides more resistance.

5.8 Static pressure distribution along the wavy wall

Wall static pressure is an important parameter in offset jet flow to characterise the flow behaviour in the recirculation region and impingement region. Figure 18 is presented to study the wall pressure variation for the present wavy surface with varying amplitudes along with the results of Pramanik and Das [44] for the plane wall surface. ~~After the exit from the nozzle, due to the presence of wall, the low pressure zone is created between jet and the wall. The pressure difference occurs and as a result of low subatmospheric pressure below the jet, the jet tilts towards the plate and attaches with the wall. This phenomenon is known as the Coanda effect [11]. The point of contact with the wall is defined as the reattachmentreattachemt point and the low sub-atmospheric pressure zone is defined as the recirculation region.~~ It is noted from the figure 18 that the pressure reaches a minimum value in the impingement region as the amplitude of the wavy surface increases as compared to Pramanik and Das [44] for the plane wall. The pressure then increases suddenly in the impingement region and attains the maximum value at the reattachment point because the velocity is

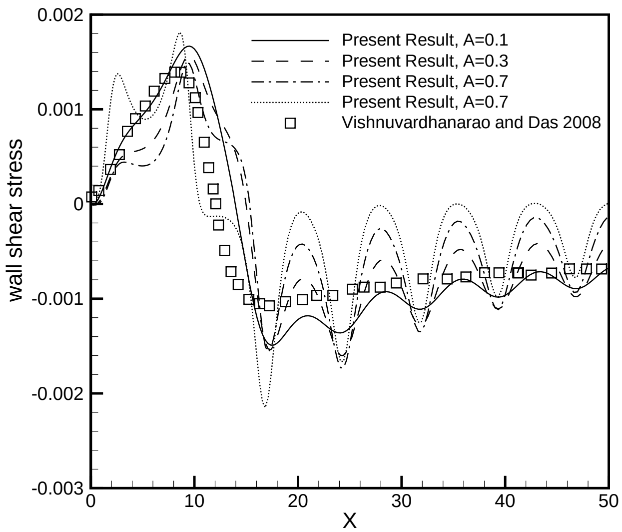

Figure 17: Variation of wall shear stress

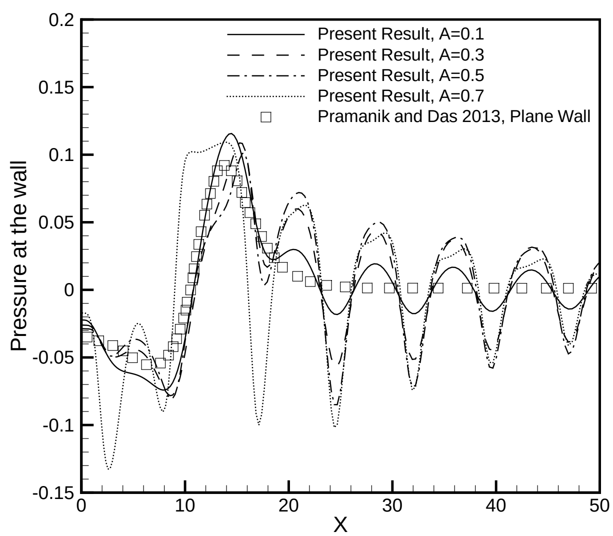

Figure 18: Variation of pressure at the wall

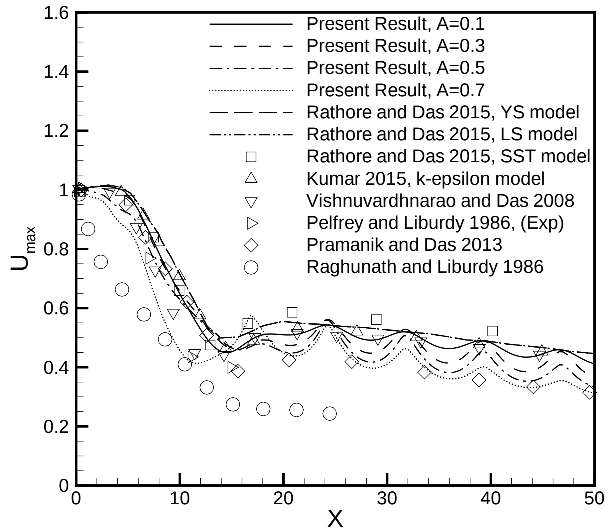

Figure 19: Decay of streamwise maximum velocity (U_{max})

zero at this point. The pressure decreases after the reattachment point and almost shows the constant value in the wall jet region for the plane wall surface. But for the wavy surface with various amplitudes, it follows the wavy pattern and the fluctuation is more for the higher value of the amplitude.

5.9 Decay in streamwise maximum velocity (U_{max}) along X

The decay in maximum streamwise velocity (U_{max}) is presented in figure 19 and also compared with the numerical results of Rathore and Das [29], Kumar [42, 41], Vishnuvardhanarao and Das [26], Pramanik and Das [44], Raghunath and~~s~~ Liburdy [47] and the experimental result of Pelfrey and Liburdy [15]. The U_{max} increases very slowly initially because of the low pressure zone in the recirculation region which accelerates the fluid. Then, the value of U_{max} decreases suddenly and attains the minimum value near the reattachment point. The reason for this variation~~On of the reason might be possible that after attending the higher value near the jet exit, the U_{max} gets affected by the viscous effects which penetrate the jet centerline. The U_{max} decreases suddenly in the recirculation region where the momentum change is occur with the vortex present in the recirculation region. Further, the vortex keeps its motion by take out the jets mean kinetic energy in the recirculation region.~~ might be that after attaining the higher value near the jet exit, the U_{max} gets affected by the viscous effects. The U_{max} decreases suddenly in the recirculation region where the momentum change takes place with the vortex present in the recirculation region. Further, the vortex utilises the kinetic energy of the jet for maintaining its motion in the recirculation region. The minimum value U_{max} is noted for the Raghunath and~~s~~ Liburdy [47]. The U_{max} increases in the impingement region where the pressure is converted into the kinetic energy and then it decreases gradually in the wall jet region. The decrease of U_{max} is higher for the higher amplitude of the wavy surface. The U_{max} follows the wavy pattern in the wall jet region for all the amplitudes of the wavy wall surface while the other results show the smooth line in the wall jet region.

5.10 Variation of jet half widths $(Y_{0.5})_1, (Y_{0.5})_2$ and Y_{max}

The spreading of the jet can be studied by measuring the jet half widths. In order to measure the jet half widths $(Y_{0.5})_1$ and $(Y_{0.5})_2$ for the present case of wavy surface, the figure 20 is presented. Here, jet half widths $(Y_{0.5})_1$ and $(Y_{0.5})_2$ indicate the upper shear layer of the offset jet and lower shear layer of the offset jet, respectively. Figure 20a shows the variation of jet half width $(Y_{0.5})_1$ of wavy surface along with the numerical results of Kumar [41] and Rathore and Das [40] for the plane wall. The definition of OR is same

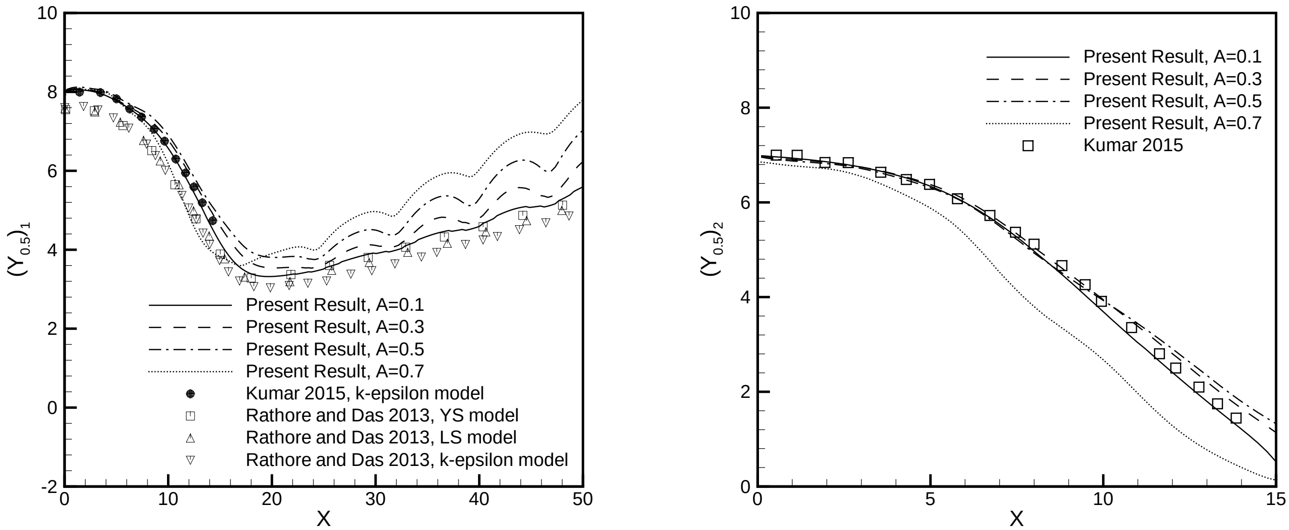

(a) Spreading of jet width $(Y_{0.5})_1$ along X axis

(b) Variation of jet width $(Y_{0.5})_2$ along X axis

Figure 20: Variation of Jet half widths $(Y_{0.5})_1$ and $(Y_{0.5})_2$ along the $X-$ direction

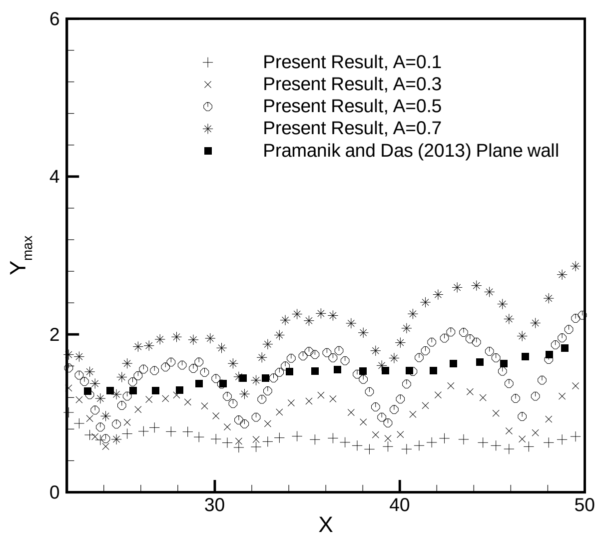

Figure 21: Variation of Y_{max} along axial direction

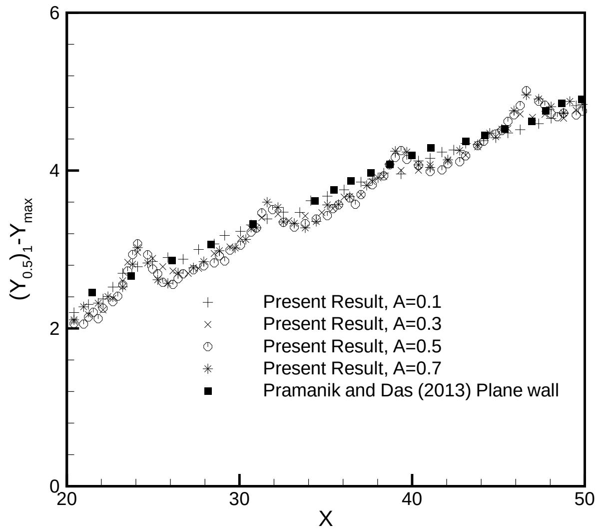

Figure 22: Growth of outer free layer along downstream distance

for present case with Kumar [41] and from present definition of OR, the offset ratio of Rathore and Das [40] is $OR = 6.5$. Figure 20b shows the variation of jet half width $(Y_{0.5})_2$ of wavy surface along with the numerical results of Kumar [41]. Figure 20a shows that the jet half width $(Y_{0.5})_1$ decreases sharply after the exit of the nozzle. The decrease is less for the higher amplitude of the wavy surface till A=0.5. But, the decrease is more for the higher amplitude, i.e. A=0.7. After the impingement~~impingment~~ region, $(Y_{0.5})_1$ increases gradually in the developing region following a wavy pattern. The waviness becomes more pronounced at higher amplitudes. On contrary to this, $(Y_{0.5})_2$ shows a smooth variation for all the amplitudes (Figure 20). Unlike $(Y_{0.5})_1$, $(Y_{0.5})_2$ decreases monotonically with increase in X.

In order to present the growth of shear layer in the wall jet region for the Y_{max} and $(Y_{0.5})_1 - Y_{max}$ are plotted in the figures 21 and 22, respectively. The Y_{max} is the lateral distance from the surface ($Y = 0$) at which the mean velocity is equal to the maximum streamwise velocity, i.e. $U = U_{max}$. In other word, Y_{max} shows the trajectory of the jet centreline. Figure 21 shows the variation in Y_{max} along the streamwise direction in the fully developed region. The Y_{max} of plane wall surface of Pramanik and Das [44] is also plotted for comparison purpose. The Y_{max} of plane wall surface increases very slowly in this region. But, it is noted that the variation in Y_{max} increases as the amplitude of the wavy surface increases and it follows the wavy pattern in the downstream direction. Figure 22 shows the growth of outer shear layer, i.e. $(Y_{0.5})_1 - Y_{max}$ for the various amplitudes in the downstream direction. Here, the variation in growth of outer shear layer of plane wall surface of Pramanik and Das [44] is also used for comparison. They mentioned that the growth rate spreads linearly in streamwise direction for plane wall surface. But, as shown in figure 22, it is noted that growth rate of each amplitude is almost same and follows the wavy pattern in the axial direction.

5.11 Variation of energy flux (E)

The variation of energy flux (E) for varying amplitudes of the wavy surface is presented in figure 23. The energy flux may be defined as the $E = \frac{1}{2}\int_{Y_{min}}^{Y_{max}} U^3 dY + \int_{Y_{min}}^{Y_{max}} P|U|dY$, in which U and P are the mean streamwise velocity and static pressure, respectively. It can be seen from figure 23 that near the exit of the jet, the energy flux (E) suddenly decreases; this continues till the recirculation region. The reason behind the decay of the energy flux ~~occurs basically~~ may be ~~the due to~~ the viscous diffusion across the jet shear layers. The energy flux suddenly decreases near the reattachment point~~recirculation~~ with increase in the amplitude of the wavy surface. It is due to the decrease in mean velocity in that region.~~might be possible that with increase in the amplitude the discontinuity in velocity occurs which may have cause the raid loss of energy.~~

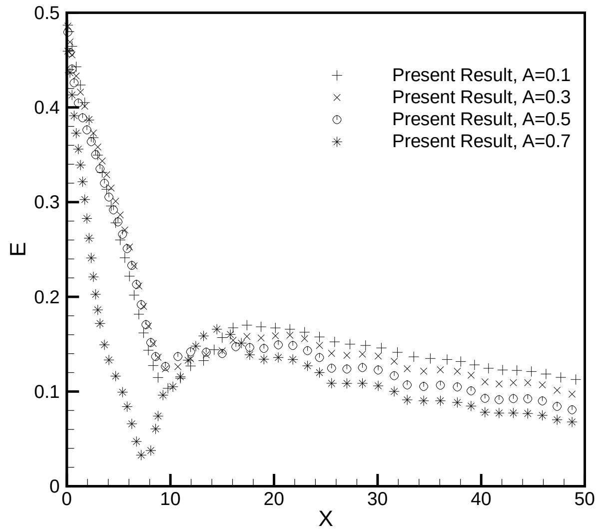

Figure 23: Variation of energy flux

The energy flux for amplitude 0.7 falls sharply than the other cases~~decay of other amplitudes~~. ~~The minimum value of decay in energy flux is obtained for the higher amplitude, i.e. 0.7 in the impingement region.~~ Then, it increases up to some downstream distance and again decreases continuously in the wall jet region. The energy flux in the wall jet region decreases as the amplitude of the wavy surface increases.

6 Conclusion

The present numerical analysis is carried out for the turbulent offset jet impinging on a wavy surface using standard $k-\varepsilon$ turbulence model. The Reynolds number and the offset ratio are consider to be $15,000$ and 7.0, respectively. The amplitude of the wavy surface is varied between $0.1 \leq A \leq 0.7$ and the number of cycle is set to 10 for all the computational study. It has been found that the vortex center of the wavy surface increases in $X-$direction and $Y-$direction when the amplitude increases but, for higher amplitude it decreases as the amplitude increases from 0.4 and 0.5 for X and Y direction, respectively. The reattachment point X_{rp} is noted maximum when the amplitude is 0.6. The minimum pressure in the recirculation region near the vortex center decreases as the amplitude of the wavy wall surface increases resulting in the increase of the magnitude of the minimum pressure $|P_{min}|$. The value of minimum pressure of wavy wall surface is very small as compared to the result of the plane wall surface. The maximum pressure near the reattachment point decreases as the amplitude increases and after $A = 0.5$, P_{max} increases. Total momentum flux is found to be maximum when the amplitude of the wavy surface is 0.6. It is noted that the momentum flux F_u increases in the recirculation region and decreases in the wall jet region as the amplitude of the wavy surface increases. The scaled similarity solution is obtained at the crest and at the trough. But, the trend is entirely different ~~diffrent~~ than the trend observed for the plane wall case. Also, it is found that the trend at the crest is different than the trend at the trough. The point of inflection is also found to move along cross~~-stream~~wise direction with the increase in the amplitude of the wavy wall. The decrease~~s~~ of the magnitude of the decay in normalized streamwise maximum velocity (U_{max}) decreases as the amplitude of the wavy surface increases. It is noted that the jet half width $(Y_{0.5})_1$ decreases sharply after the exit of the nozzle. After the impingement region, $(Y_{0.5})_1$ increases gradually in the developing region following a wavy pattern. The waviness becomes more pronounced at higher amplitudes. Unlike $(Y_{0.5})_1$, $(Y_{0.5})_2$ is found to decrease monotonically with increase in X. The present study explores the distinct features of the flow characteristics created by the wavy wall. The limitation of the present study lies with the amplitude of the wavy wall. It was noticed that for amplitude beyond 0.7, there is flow separation near the exit of the computational domain, i.e. near X=70. The standard $k-\varepsilon$ turbulence model which is used in the present work can not be used for modelling turbulence ~~model in that case~~. In that case, low Reynolds number turbulence modelling is recommended.

References

[1] N. Rajaratnam, *Turbulent jets*, Elsevier Scientific Publishing Company, (1976).

[2] C. Bourque and B. G. Newmann, Reattachment of two-dimensional incompressible jet to an adjacent plate, *Aeronaut. Quart.*, **11**, 201–232 (1960).

[3] J. Hoch and M. Jiji, Two-dimensional turbulent offset jet boundary interaction, *Journal of Fluids Engineering*, **103**(1), 154–161 (1981).

[4] T. S. Lund, Augmented thrust and mass flow associated with two-dimensional jet reattachment, *American Institute of Aeronautics and Astronautics (AIAA) Journal*, **24**(12), 1964–1970 (1986).

[5] A. Nasr and J. C. S. Lai, Comparison of flow characteristics in the near field of two parallel plane jets and an offset jet, *Physics of Fluids*, **9**(10), 2919–2931 (October 1997).

[6] J. R. R. Pelfrey and J. A. Liburdy, Effect of curvature on the turbulence of a two-dimensional jet, *Experiments in Fluids*, **4**(3), 143–149 (1986).

[7] S. K. Rathore and M. K. Das, A comparative study of heat transfer characteristics of wall-bounded jets using different turbulence models, *International Journal of Thermal Sciences*, **89**, 337–356 (2015).

[8] A. Nasr and J. C. S. Lai, Mean flow Characteristic in the near Field of a turbulent Offset jet., *Twelfth Australasian Fluid Mechanics Conference,The University of Sydney, Australia*, (1995).

[9] N. Gao, D. Ewing, and C. Y. Ching, Heat transfer in turbulent planar offset attaching jets with small initial offset distances, *International Journal of Heat and Mass Transfer*, **83**, 21–26 (2015).

[10] N. D. Castro and A. O. Demuren, Large eddy simulation of turbulent axially rotating pipe and swirling jet flows, *Proceedings of the Institute of Mechanical Engineering Part C: Journal of Mechanical Engineering Science*, **231**(9), 1749–1761 (2017).

[11] D.J. Tritton, *Physical Fluid Dynamics*, Von Norstrand Reinhold, UK, 284–286 (1977).

[12] R. A. Sawyer, The flow due to a two-dimensional jet issuing parallel to a flat plate, *Journal of Fluid Mechanics*, **9**(4), 543–559 (December 1960).

[13] R. A. Sawyer, Two-dimensional reattaching jet flows including the effects of curvature on entrainment, *Journal of Fluid Mechanics*, **17**, 481–498 (1963).

[14] N. Rajaratnam and K. Subramanya, Plane turbulent reattached wall jet, *ASCE Journal of Hydraulics Devision*, **94**(1), 95–112 (1968).

[15] J. R. R. Pelfrey and J. A. Liburdy, Mean flow characteristics of a turbulent offset jet, *Journal of Fluids Engineering*, **108**(1), 82–88 (1986).

[16] A. Nasr and J. C. S. Lai, A turbulent plane offset jet with small offset ratio, *Experiments in Fluids*, **24**, 47–57 (1998).

[17] B. E. Launder and D. B. Spalding, The Numerical Computation of Turbulent Flows, *Computer Methods in Applied Mechanics and Engineering*, **3**(2), 269–289 (1974).

[18] A.C. Benim and W. Zinser, Investigation into the finite element analysis of Confined turbulent flow using k-e model of turbulance, *Computer Methods in Applied Mechanics and Engineering*, **51**, 507–523 (1985).

[19] H. M. Koo and S. O. Park, Prediction of Turbulent Offset Jet Flows With an Assessment of QUICKER Scheme, *International Journal for Numerical Methods in Fluids*, **15**(3), 355–372 (1992).

[20] C. Fu, M. Uddin, and A. Curley, Insights derived from CFD studies on the evolution of planar wall jets, *Engineering Applications of Computational Fluid Mechanics*, **10**(1), 44–56 (2016).

[21] S. H. Chuang, Numerical Simulation of an Impinging Jet on a Flat Plate, *International Journal for Numerical Methods in Fluids*, **9**, 1413–1426 (1989).

[22] S. H. Chuang and C. Y. Wei, Computations for a jet impinging obliquely on a flat surface, *International Journal for Numerical Methods in Fluids*, **12**, 637–653 (1991).

[23] S. H. Chuang, M. H. Chen, S. W. Lii, and F. M. Tai, Numerical simulation of twin-jet impingement on a flat plate coupled with cross-flow, *International Journal for Numerical Methods in Fluids*, **14**(4), 459 – 475 (1992).

[24] S. Ashforth-Frost, K. Jambunathan, C. F. Whitney, and S. J. Ball, Heat transfer from a flat plate to a turbulent axisymmetric impinging jet, *Proceedings of the Institution of Mechanical Engineers, Part C: Journal of Mechanical Engineering Science*, **211**, 167–172 (1997).

[25] R. Dutta, A. Dewan, and B. Srinivasan, CFD study of slot jet impingement heat transfer with nanofluids, *Proceedings of the Institution of Mechanical Engineers, Part C: Journal of Mechanical Engineering Science*, **230**(2), 206–220 (2016).

[26] E. Vishnuvardhanarao and M. K. Das, Computation of Mean Flow and Thermal Characteristics of Incompressible Turbulent Offset Jet Flows, *Numerical Heat Transfer: Part A*, **53**(8), 843–869 (2008).

[27] J. T. Holland and J. A. Liburdy, Measurements of the thermal characteristics of a heated offset jets, *International Journal of Heat and Mass Transfer*, **33**(1), 69–78 (1990).

[28] H. B. Song, S. H. Yoon, and D. H. Lee, Flow and heat transfer characteristics of a two-dimensional oblique wall attaching offset jet, *International Journal of Heat and Mass Transfer*, **43**, 2395–2404 (2000).

[29] S. K. Rathore and M. K. Das, Effect of Freestream Motion on Heat Transfer Characteristics of Turbulent Offset Jet, *Journal of Thermal Science and Engineering Applications*, **8**, 011021–12 (March 2016).

[30] D. S. Kim, S. H. Yoon, D. H. Lee, and K. C. Kim, Flow and heat transfer measurements of a wall attaching offset jet, *International Journal of Heat and Mass Transfer*, **39**(14), 2907–2913 (1996).

[31] B. N. Kwakye, S. P. Clark, M. F. Tachie, J. Malenchak, and G. Muluye, Flow characteristics within the recirculation region of three-dimensional turbulent offset jet, *Journal of Hydraulic Research*, (2014).

[32] N. Mohammadaliha, H. Afshin, and B. Farahanieh, Numerical Investigation of Nozzle Geometry Effect on Turbulent 3-D Water Offset Jet Flows, *Journal of Applied Fluid Mechanics*, **9**(4), 2083–2095 (2016).

[33] A. Assoudi, S. Habli, N. M. Said, H. Bournot, and G. L. Palec, Three-dimensional study of turbulent flow characteristics of an offset plane jet with variable density, *Heat Mass Transfer*, **52**(11), 2327–2343 (November 2015).

[34] M. A. Chaab and M. F. Tachie, Characteristics of turbulent three-dimensional offset jets, *Journal of Fluids Engineering*, **133**(5), 051203–1 (2011).

[35] S. G. Kashi, R. J. Martinuzzi, and R. E. Baddour, Comparison of Far-Field Turbulent Structure of a Rectangular Surface Jet to Three-Dimensional Free and Wall Jets, *Journal of Engineering Mechanics*, **134**(3), 224–233 (March 2008).

[36] G. Biswas and V. Eswaran, *Turbulent Flows: Fundamentals, Experiments and Modeling*, Narosa Publishing House, New Delhi, India, (2002).

[37] S. V. Patankar, *Numerical Heat Transfer and Fluid Flow*, Hemisphere, New York, (1980).

[38] G. L. Stone, Iterative solution of implicit approximation of multidimensional partial differential equations, *SIAM Journal on Numerical Analysis*, **5**(3), 530–558 (1968).

[39] J. C. S. Lai and A. Nasr, Two parallel plane jets: comparison of the performance of three turbulence models, *Proceedings of the Institution of Mechanical Engineers, Part G: Journal of Aerospace Engineering*, **212**(6), 379–391 (1998).

[40] S. K. Rathore and M. K. Das, Comparison of two low Reynolds number turbulence models for fluid flow study of wall bounded jets, *International Journal of Heat and Mass Transfer*, **61**, 365–380 (2013).

[41] A. Kumar, Mean flow characteristics of a turbulent dual jet consisting of a plane wall jet and a parallel offset jet, *Computers and Fluids*, **114**, 48–65 (March 2015).

[42] A. Kumar, Mean Flow and Thermal Characteristics of a Turbulent Dual Jet Consisting of a Plane Wall Jet and a Parallel Offset Jet, *Numerical Heat Transfer, Part A*, **67**(10), 1075–1096 (2015).

[43] J. R. Pelfrey and J. A. Liburdy, Turbulence characteristics of an offset jet, *Second International symposium on applications of laser anemometry to fluid mechanics*, **1**(7), (1984).

[44] S. Pramanik and M. K. Das, Numerical characterization of a planar turbulent offset jet over an oblique wall, *Computers and Fluids*, (77), 36–55 (7 March 2013).

[45] I. Wygnanski, Y. Katz, and E. Horev, On the applicability of various scaling laws to the turbulent wall jet, *Journal of Fluid Mechanics*, **234**, 669–690 (1992).

[46] A. Kumar and M. K. Das, Study of a turbulent dual jet consisting of a wall jet and an offset jet, *Journal of Fluids Engineering*, **133**(10), 101201–11 (2011).

[47] G. Raghunath and J. A. Liburdy, Predictions of a turbulent offset jet, In *4th Fluid mechanics, plasma dynamics and lasers conference*, Vol. 1, The American Institute of Aeronautics and As!mnautics, (May 12-14 1986).